nature immunology

Article

https://doi.org/10.1038/s41590-025-02103-z

Enhancing human NK cell antitumor function by knocking out *SMAD4* to counteract TGFβ and activin A suppression

Received: 19 January 2024

Accepted: 30 January 2025

Published online: 21 March 2025

Check for updates

Anna Rea[1], Sara Santana-Hernández[2,3], Javier Villanueva[1,3], Marta Sanvicente-García[1], Mariona Cabo[2], Jesús Suarez-Olmos[2], Fabricio Quimis[2], Mengjuan Qin[2], Eduard Llorens[2], Sandra Blasco-Benito[2], Lamberto Torralba-Raga[4,5], Lorena Perez[6], Bishan Bhattarai[7], Elisenda Alari-Pahissa[2], Anna-Maria Georgoudaki[8], Francesc Balaguer[9], Manel Juan[6], Julián Pardo[10], Toni Celià-Terrassa[2,11], Ana Rovira[2,11,12], Nina Möker[13], Congcong Zhang[13], Marco Colonna[7], Jan Spanholtz[8], Karl-Johan Malmberg[4,5,14], Clara Montagut[1,2,11,12], Joan Albanell[1,2,11,12], Marc Güell[1,15], Miguel López-Botet[1,2] & Aura Muntasell[2,3,11] ✉

Transforming growth factor beta (TGFβ) and activin A suppress natural killer (NK) cell function and proliferation, limiting the efficacy of adoptive NK cell therapies. Inspired by the partial resistance to TGFβ of NK cells with *SMAD4* haploinsufficiency, we used CRISPR–Cas9 for knockout of *SMAD4* in human NK cells. Here we show that *SMAD4*^{KO} NK cells were resistant to TGFβ and activin A inhibition, retaining their cytotoxicity, cytokine secretion and interleukin-2/interleukin-15-driven proliferation. They showed enhanced tumor penetration and tumor growth control, both as monotherapy and in combination with tumor-targeted therapeutic antibodies. Notably, *SMAD4*^{KO} NK cells outperformed control NK cells treated with a TGFβ inhibitor, underscoring the benefit of maintaining SMAD4-independent TGFβ signaling. *SMAD4*^{KO} conferred TGFβ resistance across diverse NK cell platforms, including CD19-CAR NK cells, stem cell-derived NK cells and ADAPT-NK cells. These findings position *SMAD4* knockout as a versatile and compelling strategy to enhance NK cell antitumor activity, providing a new avenue for improving NK cell-based cancer immunotherapies.

Allogeneic NK cell adoptive transfer following hematopoietic stem cell transplantation exhibits promising graft-versus-leukemia efficacy and a favorable safety profile[1]. Although allogeneic NK cell therapies, including chimeric antigen receptor (CAR)-NK cells, have shown clinical benefits in certain hematological malignancies[1,2], their clinical efficacy in solid tumors remains limited[3–5], due to their inefficient homing and function in the tumor microenvironment (TME)[4,5].

Most solid tumors are poorly permeable to NK cells, partially due to the influence of TGFβ, a suppressive cytokine produced by tumor cells and other regulatory cells in the TME[6,7]. Active TGFβ binds to TGFβ type 2 receptor dimers (TGFβRII), which then recruit and activate type 1 receptors (TGFβRI) to form a tetrameric receptor complex. The canonical signaling initiates with the phosphorylation of SMAD2 and SMAD3 receptor-SMADs (R-SMADs), which subsequently complex with SMAD4 and translocate to the nucleus, where they regulate the activity of cell-type-specific transcription factors, co-activators and co-repressors[8]. Additionally, SMAD2/SMAD3 can interact with alternative partners, including transcriptional intermediary factor 1 gamma (TIF1γ or TRIM33), IKKα or DROSHA, modulating TGFβ-dependent cell proliferation and motility in hematopoietic or epithelial cells[9,10]. Beyond

A full list of affiliations appears at the end of the paper. ✉e-mail: aura.muntasell@uab.cat

https://doi.org/10.1038/s41590-025-02103-z

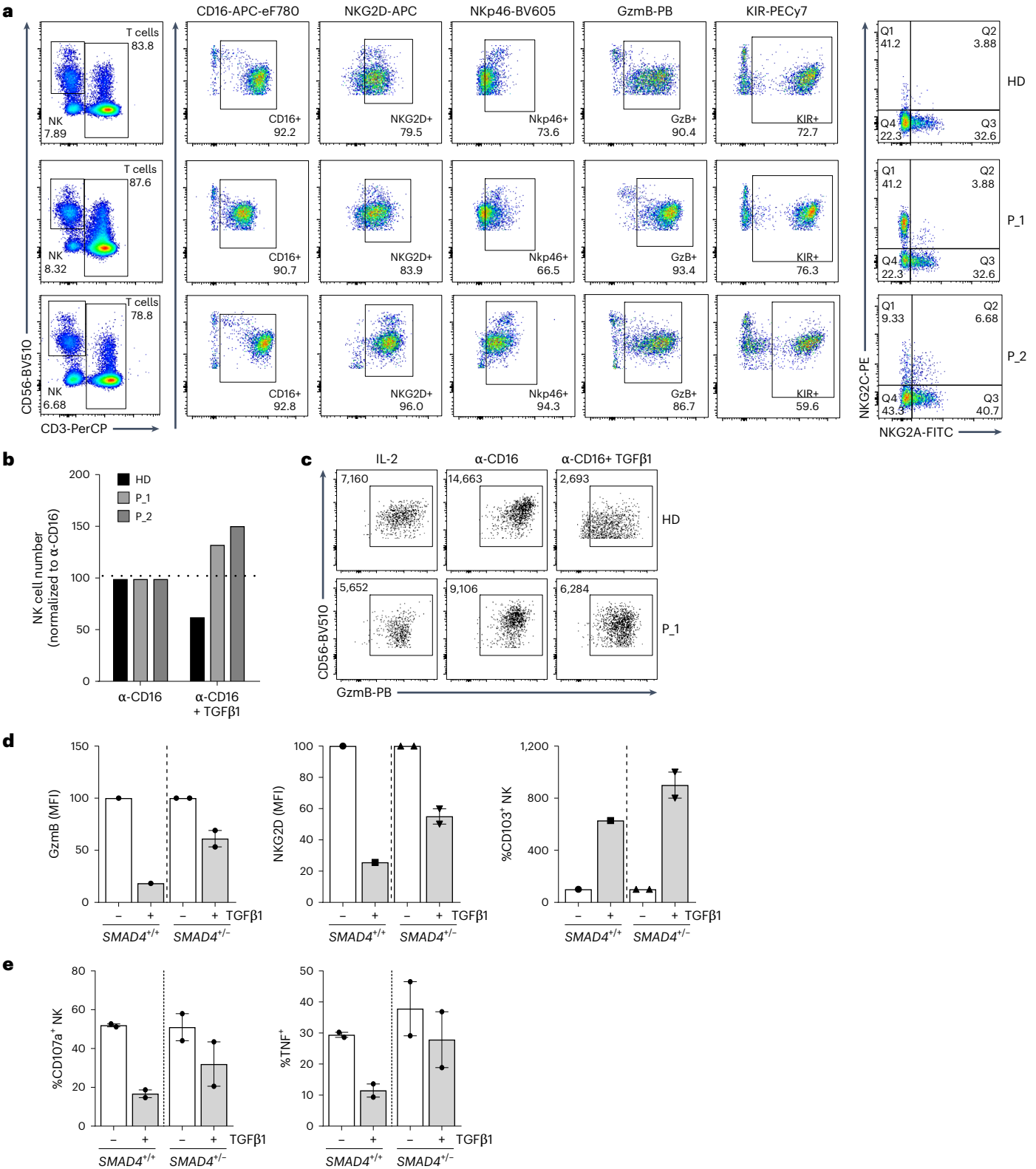

Fig. 1 | Effect of TGFβ and *SMAD4* gene dose on NK cell phenotype and function. **a**, Dot plots showing the expression of indicated markers in circulating NK cells from a healthy individual (HD) and two individuals with JPS (P_1, P_2). **b**–**d**, PBMCs were cultured on anti-CD16-coated plates with IL-2 ± TGFβ1 for 6 days. **b**, NK cell numbers at day 6. Dotted line indicates 100%. **c**, Representative dot plots of granzyme B (GzmB) expression analyzed by flow cytometry in NK cells from an HD and an individual with JPS cultured in the indicated conditions. Inset numbers indicate mean fluorescence intensity (MFI). **d**, Mean ± s.e.m. granzyme B and NKG2D fluorescence intensity and proportions of CD103$^+$ NK cells from two individuals with JPS (P, *SMAD4*$^{+/-}$) and from a healthy control (HD, *SMAD4*$^{+/+}$) at day 6, by multiparametric flow cytometry. MFI data were normalized to those of cells activated in the absence of TGFβ1. **e**, Mean ± s.e.m. degranulation (CD107a$^+$) and TNF production by NK cells from healthy donors (*SMAD4*$^{+/+}$, $n = 2$) and individuals with JPS (*SMAD4*$^{+/-}$, $n = 2$) treated or not with TGFβ1 upon 4 h coculture with K562 cells by flow cytometry. Basal CD107a and TNF NK cell values in the absence of targets were subtracted.

SMAD2/SMAD3, TGFβ can also signal through mitogen-activating protein kinases (ERK, p38 and JNK), phosphatidylinositol 3 kinase (PI3K)/Akt and small GTPases in a context-dependent manner[11]. In NK cells, TGFβ limits interferon gamma (IFNγ) production and cytotoxicity via SMAD2/SMAD3/SMAD4-dependent signaling[12–14] while inducing tissue-residency markers (for example, Hobit, CD103, CD49a and TRAIL), independently of SMAD4 (refs. 15,16). TGFβ also suppresses NK cell proliferation and the expression of activating receptors (NKp30 and NKG2D), although the signaling intermediaries remain unclear[7,17]. Besides TGFβ, SMAD4 also participates in the signaling of other members of the TGFβ superfamily, including activins and bone morphogenetic proteins (BMPs)[18]. The effects of activins and BMPs on NK cell antitumor function have been scarcely studied[19].

Numerous TGFβ pathway inhibitors have been evaluated in preclinical studies, with several advancing to clinical development[20]. However, systemic TGFβ inhibitors exhibit context and tumor-dependent effects, often requiring combination with cytotoxic treatments (for example, chemotherapy or immunotherapy), which increase the risk of adverse events[21]. Alternative approaches to circumvent TGFβ inhibition of NK cell function include preclinical studies testing the knockout of TGFβRII[22] or the expression of a dominant-negative TGFβRII by genetic engineering[23].

While *Smad4* deletion impaired NK cell maturation and homeostasis in mice, independently of TGFβ[13], heterozygous *SMAD4* loss-of-function mutation in individuals with hereditary hemorrhagic telangiectasia did not notably impact the NK cell repertoire[24]. Here, we investigated whether disrupting SMAD4 signaling in human NK cells could enhance TGFβ resistance and potentiate their antitumor efficacy by leveraging TGFβ-driven tissue-residency features.

Results

SMAD4 uncouples TGFβ inhibition from tissue residency in NK cells

Reanalysis of microarray data from CD16-activated NK cells with or without TGFβ1 (GSE156200)[7] revealed that this cytokine broadly remodeled the transcriptome of NK cells, promoting the upregulation or downregulation of 1,275 and 604 genes, respectively (Extended Data Fig. 1a). Expression of genes encoding NK cell transcription factors (*EOMES*, *PRDM1*, *TBX21*) and effector molecules (*GZMB*, *PRF1*, *IFNG*, *TNF*) was significantly downregulated (Extended Data Fig. 1b), while transcripts related to tumor homing (*CXCR3*, *CXCR4*) and tissue residency (*ZNF683*, *ITGAE*) were upregulated in CD16-activated TGFβ1-treated NK cells (Extended Data Fig. 1c). Downregulated pathways included cytokine signaling, cell migration, cell killing and cell activation, whereas TGFβ1 promoted pathways related to cell adhesion, chemotaxis and leukocyte differentiation (Extended Data Fig. 1d).

To define the SMAD4-specific role in mediating TGFβ effects, we examined NK cells from two individuals with juvenile polyposis syndrome (JPS) with *SMAD4* haploinsufficiency and investigated the impact of TGFβ treatment on their functional activity. Western blot analysis confirmed reduced SMAD4 expression in their peripheral blood mononuclear cells (PBMCs; Extended Data Fig. 2a,b). NK cell proportions and $CD56^{hi}$ or $CD56^{lo}$ subset distribution, along with expression of main receptors (CD16, NKG2D, NKG2A, KIR) and granzyme B were comparable to healthy controls (Fig. 1a). One individual showed an expansion of human cytomegalovirus (HCMV)-induced adaptive $NKG2C^{+}$ NK cells (Fig. 1a). Unlike $SMAD4^{+/+}$ NK cells from a control individual, TGFβ1 treatment did not reduce $SMAD4^{+/-}$ NK cell numbers 6 days after CD16 activation (Fig. 1b). Furthermore, TGFβ-induced downregulation of NKG2D and granzyme B was less pronounced in CD16-activated $SMAD4^{+/-}$ compared to $SMAD4^{+/+}$ NK cells, whereas the acquisition of CD103 was maintained (Fig. 1c,d and Extended Data Fig. 2c–e). Remarkably, $SMAD4^{+/-}$ and $SMAD4^{+/+}$ NK cells showed comparable degranulation and TNF when cocultured with the HLA-I-negative erythroleukemic cell line K562. However, upon treatment with TGFβ1, NK cells from individuals with JPS showed higher functionality compared to controls (Fig. 1e).

Together, these results indicate that TGFβ canonical signaling suppresses human NK cell effector function while promoting tissue-residency markers, pointing to SMAD4 as the molecular switch where these pathways diverged.

Efficient $SMAD4^{KO}$ in human NK cells using Cas9-RNP

We hypothesized that reducing SMAD4 in primary NK cells would modulate their TGFβ sensitivity, enhancing their antitumor activity and tumor homing. The experimental strategy for the generation of primary $SMAD4^{KO}$ NK cells involved: (i) initial NK cell expansion with the irradiated 8866 lymphoblastoid cell line; (ii) on day 7, isolation and nucleofection of NK cells with Cas9–trRNA-ATTO550/CRISPR RNA (crRNA) *SMAD4* exon5 or Cas9–trRNA-ATTO550 as a control; and (iii) use of TGFβ1 as a selective pressure in the second phase of expansion (day 7–14) for reducing the proliferation of non-engineered NK cells while enriching in $SMAD4^{KO}$ NK cells (Fig. 2a). The average Cas9–guide RNA (gRNA) ribonucleoprotein (RNP) nucleofection efficiency was of 86% (Extended Data Fig. 3a,b), inducing a homogeneous reduction of 40% to 70% of SMAD4 amount in expanded NK cells as determined by flow cytometry and western blot, respectively (Fig. 2b–d and Extended Data Fig. 3c). TGFβ1 addition had no substantial effect on SMAD4 levels in control NK cells, whereas levels tended to decrease in $SMAD4^{KO}$ NK cells, suggesting a positive selection of $SMAD4^{KO}$ cells by the pressure of TGFβ (Fig. 2c,d). $SMAD4^{KO}$ and control-engineered NK cells showed comparable levels of TGFβRII, TIF1γ and SMAD7. TGFβ1-induced phosphorylation of SMAD2/SMAD3 was maintained in $SMAD4^{KO}$ NK cells, indicating functional proximal TGFβ signaling (Fig. 2c,d).

To assess *SMAD4* CRISPR efficiency, we sequenced an amplimer covering the targeted region in NK cells from three individuals. Edited allele frequencies were 71%, 57% and 74% without TGFβ1 treatment, rising to 79%, 72% and 79% with TGFβ selection during expansion (Fig. 2e). Most mutations involved insertions and deletions generating out-of-frame transcripts. Genotype frequency estimates for bulk NK cell population indicated 67%, 43% and 72% $SMAD4^{-/-}$; 30%, 46% and 26% $SMAD4^{+/-}$ and only 3%, 10% and 2% $SMAD4^{+/+}$ cells after engineering. TGFβ selection reduced $SMAD4^{+/+}$ while increasing the proportion of $SMAD4^{-/-}$ NK cells (Fig. 2f). Three common and prevalent

Fig. 2 | Efficiency of $SMAD4^{KD}$ by CRISPR–Cas9 in in vitro expanded human NK cells. a, PBMCs from healthy donors were expanded with irradiated 8,866 feeder cells. At day 7, NK cells were isolated and nucleofected with either *SMAD4* gRNA or control (CTRL) Cas9–gRNA RNP. After overnight culture, cells were further expanded in the presence of IL-2 ± TGFβ1 for 6 days. **b**, Mean ± s.e.m. SMAD4 expression by intracellular flow cytometry in control and $SMAD4^{KO}$ NK cells cultured or not with TGFβ1 ($n = 6$). **c**,**d**, TGFβ canonical signaling molecules in control NK and $SMAD4^{KO}$ NK cells by western blot. **c**, Representative western blots for TGF-BRII, pSMAD2, SMAD4, TIF1γ, SMAD7 and β-actin. **d**, Quantification of western blot data from three independent engineering experiments with cells from different donors. Bar graphs show the mean ± s.e.m. **e**–**h**, Cas9-targeted sequence in *SMAD4* was amplified by PCR, sequenced by Illumina and analyzed against the reference sequence. Data from engineered NK cells from three individuals in three independent experiments (D1, D2, D3). **e**, Allelic frequencies of out-of-frame (OUT) and in-frame (IN) indels in the presence/absence of TGFβ1. **f**, *SMAD4* genotype frequencies estimated by the Hardy–Weinberg principle in the presence or absence of TGFβ1. **g**, Allelic frequencies of the three predominant *SMAD4* mutated alleles found in NK cells from all three individuals. Horizontal dashed line in **e** and **g** indicates 50%. **h**, The three most common mutations found in *SMAD4* exon 5. Black outlines indicate the number of nucleotides inserted or deleted in the SMAD4 exon 5 and the exact nucleotide site where the mutation is found. Statistical significance by one-way analysis of variance (ANOVA) followed by Tukey's multiple-comparisons test for **b** and **d**. WT, wild type.

https://doi.org/10.1038/s41590-025-02103-z

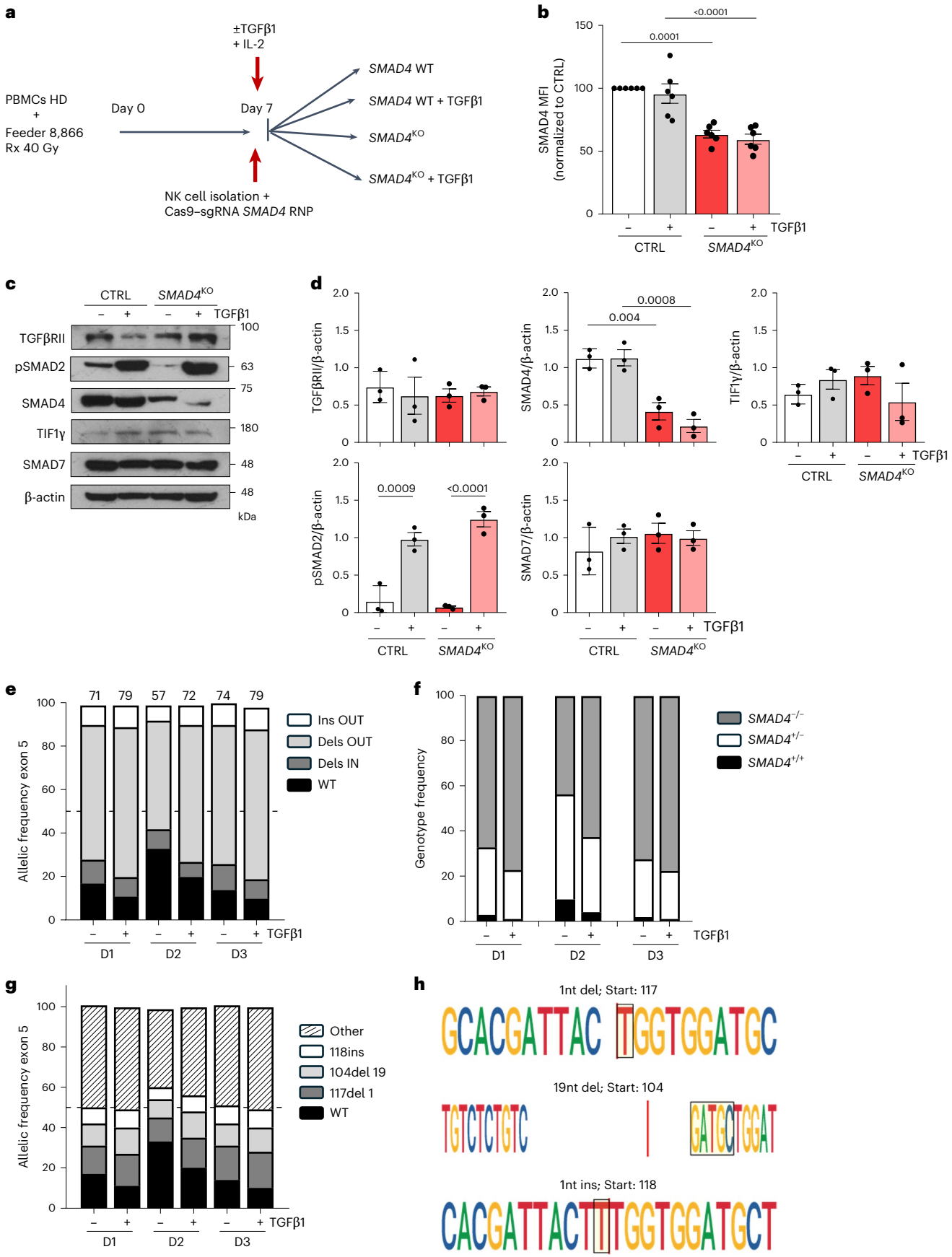

out-of-frame mutations (one thymidine deletion at position 117, one thymidine insertion at position 118, and a 19-nucleotide deletion at position 104) were found (Fig. 2g), consistent with non-homologous end-joining and microhomology-mediated end-joining DNA repair mechanisms (Fig. 2h).

We did not detect off-target events considering differentially expressed genes (DEGs) in bulk RNA-sequencing (RNA-seq) analysis with the CRISPRroots tool[25]. Alignment of the crRNA revealed three potential off-target genomic variants—*CREBBP*, *DCTN5* and *NUFIP2*—athough amplification and sequencing in control and *SMAD4*^{KO} NK cells revealed no mutations in these regions (Extended Data Fig. 4).

These data confirm the efficiency, specificity and safety of this *SMAD4* engineering approach in human NK cells, while showing preserved early TGFβ signaling in *SMAD4*^{KO} cells.

SMAD4^{KO} NK cells are functional and proliferate despite TGFβ

Deletion of *Smad4* has been shown to impair mouse NK cell maturation and homeostasis, independently of TGFβ[13]. Analysis of bulk RNA-seq data showed that the global transcriptomic profiles of *SMAD4*^{KO} and control expanded NK cells were remarkably similar, with only 53 DEGs (Fig. 3a). *SMAD4*^{KO} NK cells exhibited lower expression of *SMAD4*, *CD160* and *CD226* (DNAM-1) transcripts, alongside increased levels of *IL9R* and *ZNF683* (Hobit; Fig. 3b). The 39 genes downregulated in *SMAD4*^{KO} NK cells clustered in two biological networks related to transcriptional activity of SMAD2/SMAD3/SMAD4 and eukaryotic translation initiation (Extended Data Fig. 5). In contrast, TGFβ1 exposure altered the expression of 3,787 genes in control NK cells, while only 1,091 transcripts were affected in *SMAD4*^{KO} NK cells (Fig. 3a). TGFβ-dependent downregulation of several granzymes, activating receptors, signaling adaptors, integrins and chemokine and cytokine receptors was attenuated in *SMAD4*^{KO} NK cells (Fig. 3c–e), which retained a transcriptomic profile akin to that of activated NK cells, despite TGFβ1 treatment (Fig. 3f).

Flow cytometry analysis confirmed that in homeostatic conditions, control NK and *SMAD4*^{KO} NK cells displayed comparable levels of granzyme B, perforin-1 and several activating receptors (CD16, NKG2D, NKp30; Fig. 3g and Extended Data Fig. 6a). However, the reduction of SMAD4 significantly prevented the downregulation of NKG2D, CD16, NKp30, granzyme B and perforin-1 induced by TGFβ1 treatment (Fig. 3g and Extended Data Fig. 6a). Of note, knocking out *SMAD4* did not significantly alter the expression and distribution of HLA-I-specific inhibitory receptors (KIR, NKG2A) and differentiation markers (NKG2C, CD57 and KLRG1) in primary expanded NK cells (Fig. 3h and Extended Data Fig. 6b).

TGFβ inhibits NK cell proliferation. Given that transcripts for expression of *IL15RA*, *IL2RG* and *IL2RA* were higher in *SMAD4*^{KO} NK cells exposed to TGFβ1 compared to controls (Fig. 3i), we assessed whether *SMAD4*^{KO} NK cells could proliferate in response to interleukin (IL)-2/IL-15 despite the presence of TGFβ1. CFSE-labeled NK cells were activated via NKp46, one of the few activating receptors unaffected by TGFβ, in the presence of the pro-proliferative cytokine IL-2. In contrast to the inhibitory effects in control NK cells, *SMAD4*^{KO} NK cells, displayed enhanced proliferation when exposed to IL-2 and TGFβ1 combination (Fig. 3j,k). Analogously, the expansion of *SMAD4*^{KO} NK cells with K562-CD137L-IL15tmb-IL21tmb feeder cells was sustained in the presence of TGFβ1, while it was significantly reduced in control NK cells (Fig. 3l). Of note, knockout of *SMAD4* did not alter the proliferative capacity nor the phenotype of NK cells along time in homeostatic conditions (Fig. 3j,l and Extended Data Fig. 6c,d).

In summary, knockout of *SMAD4* in human expanded NK cells did not negatively impact granzyme B levels, maturation status or transcriptomic profile, aligning with observations from NK cells of *SMAD4*$^{+/-}$ individuals with JPS. Of interest, the reduction in SMAD4 levels partially prevented the downregulation of activating receptors and cytotoxic effectors induced by TGFβ in NK cells and preserved their proliferation in response to IL-2 and IL-15.

SMAD4^{KO} NK cells show enhanced antitumor function

We next assessed the antitumor activity of *SMAD4*^{KO} NK cells against the colorectal cancer cell line HCT116. In the absence of TGFβ1, both control and *SMAD4*^{KO} NK cells showed comparable cytotoxicity. However, TGFβ1 treatment significantly reduced the cytotoxicity of control NK cells, while *SMAD4*^{KO} NK cells maintained their killing capacity (Fig. 4a). Notably, *SMAD4*^{KO} NK cells also maintained the secretion of CCL5, IFNγ and TNF despite TGFβ1 exposure, in contrast to the reduction in control NK cells (Fig. 4b,c and Extended Data Fig. 7a). To analyze the ability for serial killing, we cocultured PKH26-labeled NK cells with HCT116-GFP^{+}Luc^{+} spheroids. Control NK cells treated with TGFβ1 accumulated in the spheroid periphery and showed reduced spheroid growth control. In contrast, TGFβ1-treated *SMAD4*^{KO} NK cells demonstrated enhanced spheroid killing, achieving levels comparable to those of NK cells not exposed to TGFβ1 (Fig. 4d–f and Extended Data Fig. 7b).

We next evaluated the antitumor function of *SMAD4*^{KO} NK cells in two humanized models of HER2-positive breast and colorectal cancers, using HCC1954 and HCT116 xenografts in NSG mice. Subcutaneously implanted tumors were treated with control or *SMAD4*^{KO} NK cells either as monotherapy (both models) or in combination with anti-HER2 antibodies (trastuzumab and pertuzumab) to assess antibody-dependent cytotoxicity (HCC1954 xenografts). NK cells were injected intratumorally once a week for 3 weeks and supported by intraperitoneal IL-2 administration every 3–4 days. HER2 antibodies were co-administered intraperitonially with IL-2 (Fig. 4g).

In the HCC1954 model, tumor growth kinetics in mice treated with control NK cells were comparable to those treated with anti-HER2 alone as a control group (Fig. 4h and Extended Data Fig. 7c). Tumor growth was significantly reduced when control NK cells in were combined with anti-HER2, demonstrating a synergistic effect (Fig. 4h and Extended Data Fig. 7c). Remarkably, *SMAD4*^{KO} NK cells provided superior tumor growth control, both as monotherapy and in combination with anti-HER2, surpassing the efficacy of control NK cells in both contexts (Fig. 4h and Extended Data Fig. 7c). In the HCT116 model, the advantage of *SMAD4*^{KO} NK cells over control NK cells in controlling tumor growth

Fig. 3 | TGFβ-dependent and -independent effects of SMAD4 in human expanded NK cell transcriptome and phenotype. a–**f**, Average changes in gene expression between control and *SMAD4*^{KO} NK cells from three different donors. **a**, Number of DEGs between indicated conditions (*P* value < 0.01). **b**, DEGs between control and *SMAD4*^{KO} NK cells ± TGFβ1. Red dots indicate significant DEGs. **c**–**e**, Expression of selected genes related to NK cell receptors and signaling adaptors (**c**), NK cell effector molecules (**d**) and soluble mediators (**e**). **f**, Gene-set enrichment analysis (GSEA) of RNA-seq data from control and *SMAD4*^{KO} NK cells treated with TGFβ1 against liver and intestine CD56^{lo} NK/type 1 innate lymphoid cells (ILC1; GSE37448). NES, normalized enrichment score. **g**, Mean ± s.e.m. expression of surface NKG2D (*n* = 11), CD16 (*n* = 7), NKp30 (*n* = 5) and intracellular GzmB (*n* = 9) and perforin-1 (*n* = 6) in control and *SMAD4*^{KO} NK cells ± TGFβ1 by flow cytometry. Dots show data from independent experiments. **h**, Mean percentage of cells positive for NKp46, KIR, NKG2A, NKG2C, CD57 and KLRG1 in control NK and *SMAD4*^{KO} NK cells ± TGFβ1 by flow cytometry. Asterisks label significant differences in control NK cells in the absence of TGFβ1 (NT). **i**, Expression of IL2 and IL15 receptor transcripts in control and *SMAD4*^{KO} NK cells by bulk RNA-seq. **j**,**k**, IL-2-driven proliferation of NKp46-activated, CFSE-labeled control and *SMAD4*^{KO} NK cells in the presence or absence of TGFβ1 by flow cytometry. **j**, Data are from one representative experiment. The vertical dashed line indicates the lowest CFSE labeling at day 0, for helping in the visualization of differences between conditions. **k**, Mean ± s.e.m. percentage of divided cells at day 6. Statistical significance by one-way ANOVA test. **l**, Control and *SMAD4*^{KO} NK cells were expanded with K562-CD137L-IL15tmb-IL21tmb feeder cells for 7 days with IL-2 ± TGFβ1. Median, minimum and maximum NK cell expansion fold at day 7 in each culture condition. Statistical significance by two-tailed moderated *t*-test in **a** and **b**, one-way ANOVA followed by Tukey's multiple-comparisons test in **g**, and one-way ANOVA followed by uncorrected Fisher's test in **k** and **l**. FC, fold change.

https://doi.org/10.1038/s41590-025-02103-z

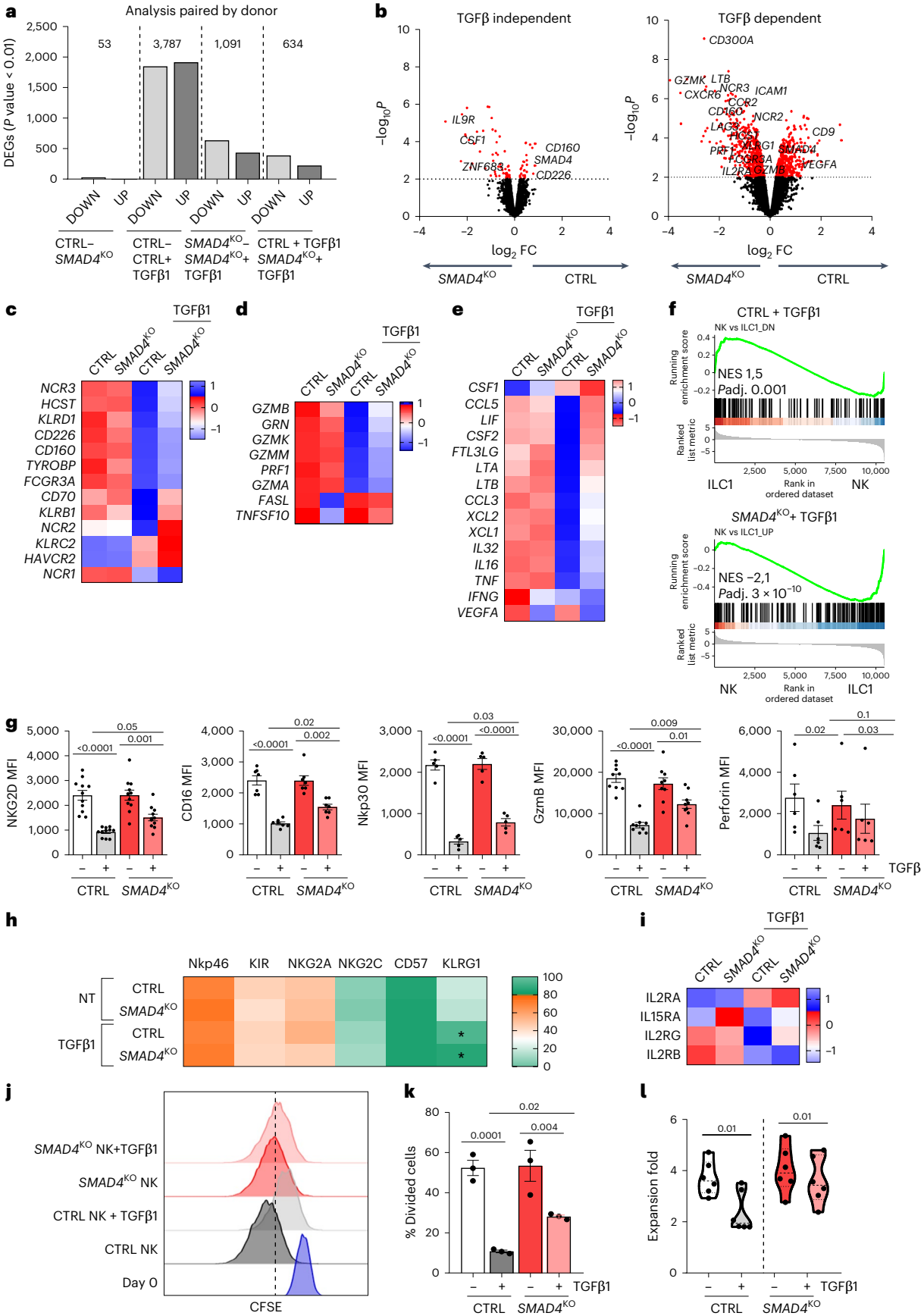

https://doi.org/10.1038/s41590-025-02103-z

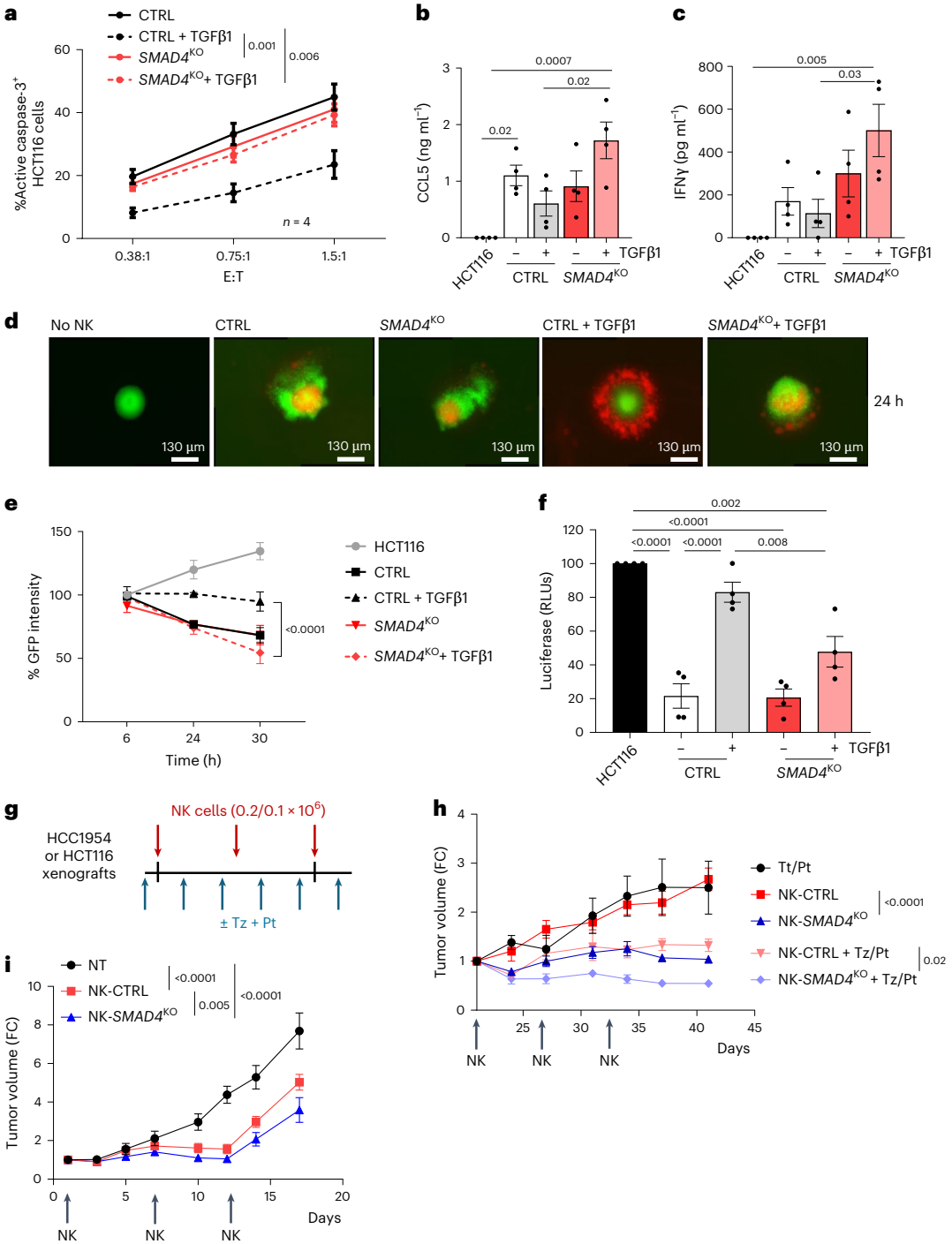

Fig. 4 | In vitro and in vivo *SMAD4*^{KO} NK cells antitumor function. **a**, Mean ± s.e.m. percentage of activated caspase-3-positive HCT116 cells after coculture with control NK and *SMAD4*^{KO} NK cells treated with IL-2 ± TGFβ1 at the indicated effector:target (E:T) ratios analyzed by flow cytometry. Spontaneous active caspase-3 levels were subtracted. Data are from four independent experiments. **b**,**c**, Amount of CCL5 (**b**) and IFNγ (**c**) in cell-free culture supernatants of control NK and *SMAD4*^{KO} NK cells after coculture with the HCT116 cell line by ELISA. Each dot shows data from an independent experiment ($n = 4$). **d**–**f**, HCT116-GFP^{+}-Luc^{+} spheroids were cocultured with PKH26-labeled control NK or *SMAD4*^{KO} NK cells previously exposed or not to TGFβ1. Images were taken at 6 h and 24 h. **d**, Representative image of one spheroid in each coculture at 24 h. **e**, Mean ± s.e.m. GFP intensity along time in each coculture. Data are from two independent experiments including five technical replicates each. Only the significance by two-way ANOVA followed by Tukey's multiple-comparisons test between TGFβ1-treated control and SMAD4^{KO} NK cells at 30 h is indicated. **f**, Mean ± s.e.m. luciferase activity of remaining HCT116 spheroids after 24 h of coculture with NK cells. Each dot represents the average cytotoxic activity of NK cells in four independent experiments. **g**,**h**, Tumor growth kinetics of HCC1954 xenografts in NSG mice treated with: (i) trastuzumab (Tz)/pertuzumab (Pt) ($n = 4$); (ii) control NK cells (2×10^5, $n = 5$); (iii) *SMAD4*^{KO} NK cells (2×10^5, $n = 5$); (iv) control NK cells (1×10^5) and trastuzumab/pertuzumab ($n = 5$); or (v) *SMAD4*^{KO} NK cells (1×10^5) and trastuzumab/pertuzumab ($n = 5$). **g**, Treatment schedule. **h**, Tumor volume fold change in each treatment group. Only differences between control and *SMAD4*^{KO} NK cells at last measurement are indicated. **i**, Tumor growth kinetics of HCT116 xenografts in NSG mice treated with either control or *SMAD4*^{KO} NK cells (2×10^5). Tumor volume fold change in each treatment group ($n = 5$ in NT group, $n = 6$ in control and *SMAD4*^{KO} NK cell groups). Statistical significance by two-way ANOVA followed by Tukey's multiple-comparisons test at last measurement for **a**, **e**, **h** and **i**; and one-way ANOVA followed by Tukey's multiple-comparisons test for **b**, **c**, **f** and **g**. RLUs, relative light units.

https://doi.org/10.1038/s41590-025-02103-z

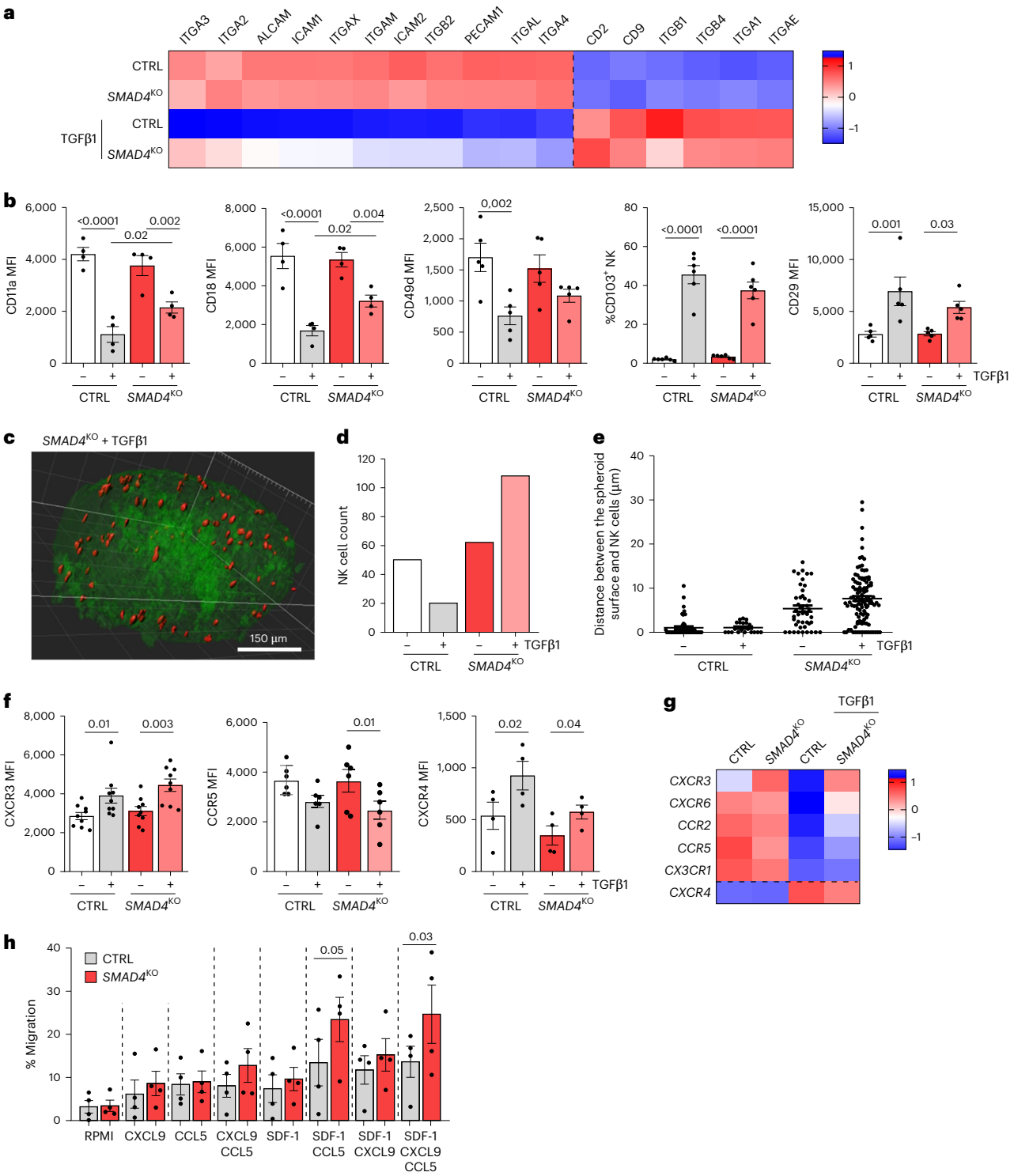

Fig. 5 | The impact of of SMAD4 and TGFβ in the integrin profile, tumor penetrance and transmigration of NK cells. a, Mean transcript levels of adhesion molecules by RNA-seq analysis. **b**, Mean ± s.e.m. percentage or intensity of surface expression levels of CD11a ($n = 4$), CD18 ($n = 3$), CD49d ($n = 5$), CD103 ($n = 6$) and CD29 ($n = 5$) by flow cytometry in control and *SMAD4*^{KO} NK cells treated or not with TGFβ1. Each dot indicates the results from an independent experiment with NK cells from different individuals. **c**–**e**, HCT116 spheroids were cocultured with control NK or *SMAD4*^{KO} NK cells previously exposed or not to TGFβ1. After 1 h coculture, spheroids and attached NK cells were fixed and processed for light-sheet imaging. HCT116 cells were labeled with an anti-EpCAM-FITC antibody and NK cells with an anti-CD45-Vio R667. **c**, Image of a representative HCT116 spheroid (green surface) cocultured with *SMAD4*^{KO} NK cells (red dots). **d**, Number of NK cells counted in spheroids in the indicated conditions. **e**, Quantification of the distance between the spheroid surface and each infiltrating NK cell. Each dot represents the measurement of one infiltrating NK cell in one experiment. **f**, Mean ± s.e.m. fluorescence intensity of surface CXCR3 ($n = 9$), CCR5 ($n = 6$) and CXCR4 ($n = 4$) in control and *SMAD4*^{KO} NK cells treated or not with TGFβ1 by flow cytometry. Each dot shows data from independent experiments. **g**, Transcript expression levels of chemokine receptors in control NK and *SMAD4*^{KO} NK cells exposed or not to TGFβ1, according to RNA-seq data from three independent donors. The dashed lines in **a** and **g** separate genes downregulated from those upregulated by TGFβ in control NK cells. **h**, Mean ± s.e.m. percentage of transmigrating control or *SMAD4*^{KO} NK cells treated with TGFβ1 to CCL5, CXCL9, SDF-1/CXCL12 or the indicated chemokine combinations. Data are from four independent experiments with NK cells from different donors. In all assays, statistical significance was calculated by one-way ANOVA followed by Fisher's test.

https://doi.org/10.1038/s41590-025-02103-z

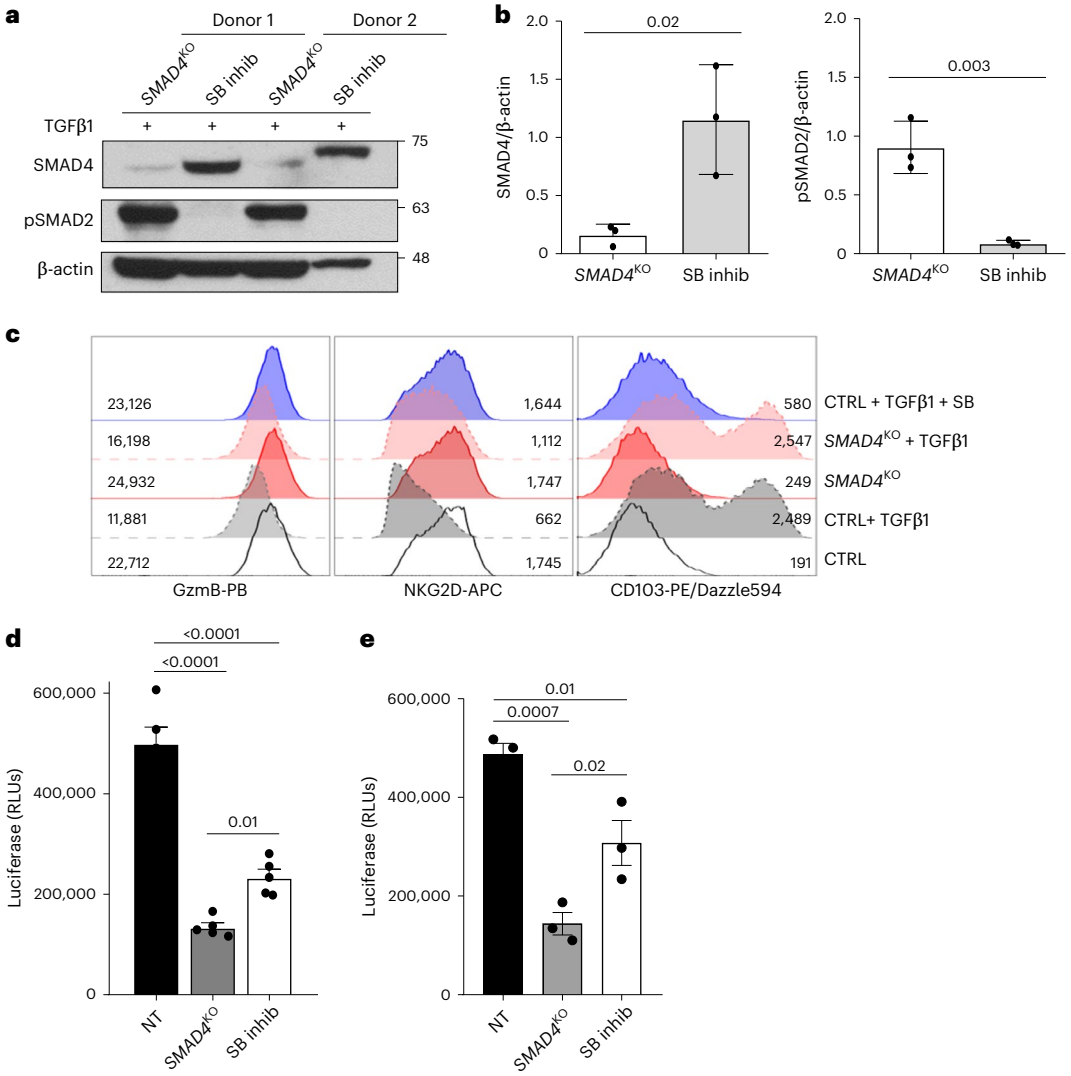

Fig. 6 | *SMAD4*^{KO} NK cells display superior cytotoxicity than control NK cells treated with a TGFBR-I inhibitor. a–**d**, *SMAD4*^{KO} and control NK cells were expanded in the presence of TGFβ1 for 7 days. Control NK cells were treated with the TGFBR-I inhibitor SB-431542 (SB inhib). **a**,**b**, SMAD4, pSMAD2 and β-actin levels in total cell extracts by western blot in *SMAD4*^{KO} and control NK cells. **a**, Representative western blots including NK cells from two different donors. **b**, Quantification of mean ± s.e.m. levels of SMAD4/β-actin and pSMAD2/β-actin ratios in NK cells from three different donors. Statistical significance was calculated by a two-tailed, unpaired Student's *t*-test. **c**, Representative histograms showing the expression of GzmB, NKG2D and CD103 in the indicated NK cells by flow cytometry. **d**,**e**, *SMAD4*^{KO} and control NK cells treated with SB-431542 were cocultured with HCT116-GFP^{+}-Luc^{+} spheroids. Luciferase counts were analyzed at 24 h of coculture. **d**, Mean ± s.e.m. luciferase counts from one representative experiment. Dots show data from five technical replicates. **e**, Mean ± s.e.m. luciferase counts from three independent experiments using NK cells from different individuals. Each dot indicates the mean of five technical replicates for each condition/experiment. Statistical significance was calculated by one-way ANOVA followed by Tukey's multiple-comparisons test for **d** and **e**.

was less pronounced (Fig. 4i and Extended Data Fig. 7d), despite their enhanced cytotoxicity against HCT116 tumor spheroids in vitro (Fig. 4d–f and Extended Data Fig. 7b). The aggressive growth of HCT116 tumors and their resistance to IFN-mediated cell death likely accounted for the relatively small differences observed in vivo (Extended Data Fig. 7e).

Our findings demonstrate that knocking out *SMAD4* in human expanded NK cells had no impact on their cytotoxicity or cytokine production in homeostatic conditions, while preventing TGFβ inhibition of NK cell cytotoxicity and cytokine production, resulting in superior antitumor activity both in vitro and in vivo.

Tumor spheroid infiltration and migration of *SMAD4*^{KO} NK cells

The two biological pathways preferentially upregulated by TGFβ in NK cells were cell adhesion and chemotaxis (Extended Data Fig. 1d). *SMAD4*^{KO} NK cells were partially resistant to the TGFβ1-induced downregulation of several adhesion molecules, including *ITGA2* (CD49b), *ITGB2* (CD18), *ITGAL* (CD11a), *ITGAM* (CD11b), *ICAM1* (CD54), *ICAM2* (CD102), *PECAM1* (CD31) and *ITGA4* (CD49d), at both mRNA and protein levels, while no differences were detected in basal conditions (Fig. 5a,b). On the other hand, these cells preserved the sensitivity to the TGFβ1-mediated upregulation of tissue-residency integrins, such as ITGB1 (CD29), ITGA1 (CD49a), and ITGAE (CD103; Fig. 5a,b and Extended Data Fig. 8a). To assess whether the enhanced expression of adhesion molecules influenced NK cell tumor infiltration, NK cells were cocultured with HCT116 spheroids for 1 h and analyzed by light-sheet microscopy (Fig. 5c and Extended Data Fig. 8b). Although similar numbers of control and *SMAD4*^{KO} NK cells were counted within spheroids (n = 51 and 63, respectively), *SMAD4*^{KO} NK cells penetrated deeper (mean distance from the spheroid surface (min–max) = 1.02 (0–11) µm and 5.3 (0–16) µm, respectively; Fig. 5c–e). Remarkably, TGFβ1 treatment significantly enhanced *SMAD4*^{KO} NK cell binding (n = 109) and penetration

https://doi.org/10.1038/s41590-025-02103-z

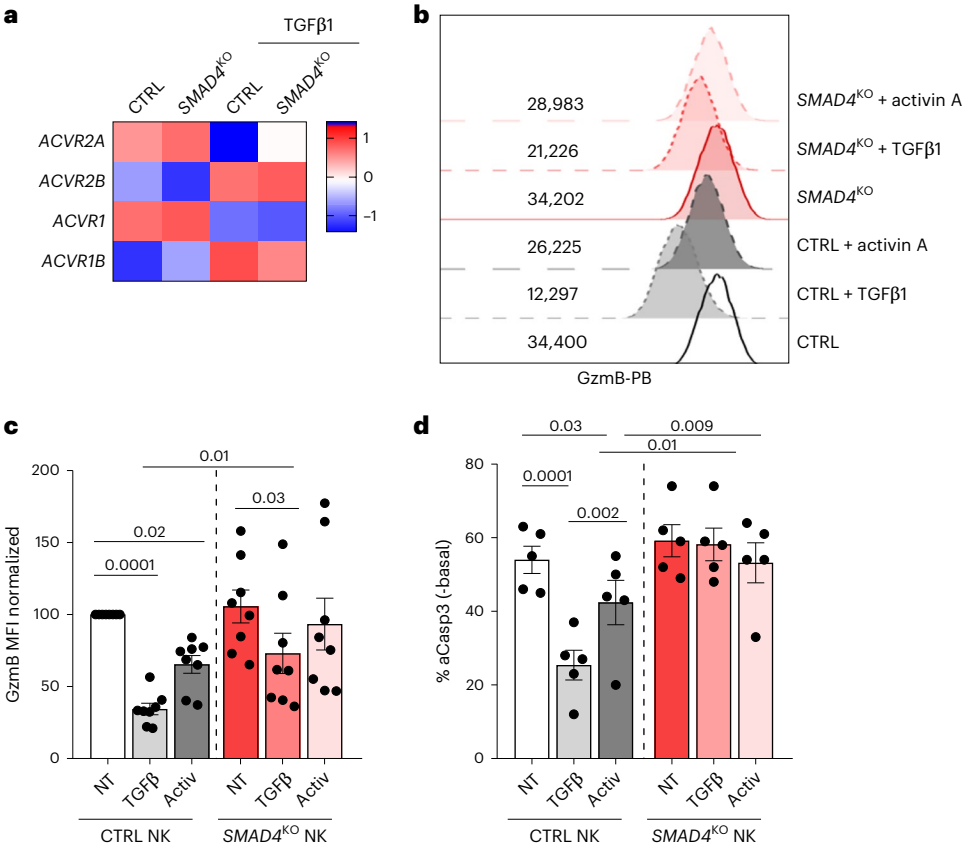

Fig. 7 | The effect of activin A in control and *SMAD4*^{KO} NK cells. a, Relative transcript expression of activin receptor genes in the indicated NK cells. Average expression in NK cells from three independent individuals as analyzed by RNA-seq. **b**–**d**, *SMAD4*^{KO} and control NK cells were incubated with TGFβ1 or activin A for 7 days. **b**, Expression of GzmB at day 7 by flow cytometry. **c**, Mean ± s.e.m. granzyme B levels in *SMAD4*^{KO} and control NK cells. Data are from experiments with NK cells from eight different individuals. **d**, *SMAD4*^{KO} and control NK cells previously incubated with TGFβ1 or activin A (Activ) were cocultured with HCT116 cells for 2 h. Mean ± s.e.m. percentage of active caspase-3^{+} (aCasp3) HCT116 cells in the indicated conditions. Data are from five independent experiments with NK cells from different individuals. Statistical significance was calculated by one-way ANOVA followed by Fisher's test.

into tumor spheroids (mean distance (min–max) = 7.6 (0–30) µm) while severely impairing control NK cells (n = 21; mean distance (min–max) = 1.07 (0–3) µm; Fig. 5c–e). In addition to adhesion molecules, TGFβ1 reduced CCR5 while upregulating CXCR3 and CXCR4 expression in both control NK and *SMAD4*^{KO} NK cells (Fig. 5f,g). Despite similar chemokine receptor profiles, *SMAD4*^{KO} NK cells treated with TGFβ1 showed enhanced migration toward CXCL12 (SDF-1) in combination with CCL5 and CXCL9, compared to TGFβ1-treated control NK cells (Fig. 5h). In summary, human *SMAD4*^{KO} NK cells maintained their anti-tumor function and proliferative potential while exhibiting enhanced tumor-homing and infiltration in the presence of TGFβ.

SMAD4^{KO} NK cells are more cytotoxic than TGFβ inhibitor-treated NK cells

Given its suppressive role in the TME, several strategies blocking TGFβ activity have been explored in preclinical and early-phase clinical studies[22,23]. We compared the cytotoxic activity of *SMAD4*^{KO} NK cells treated with TGFβ1 to that of control NK cells treated with TGFβ1 in the presence of SB-431542, a selective inhibitor of TGFβRI kinase activity[26]. The addition of SB-431542 during the expansion phase with TGFβ1 effectively precluded SMAD2 phosphorylation, without affecting SMAD4 expression (Fig. 6a,b). As expected, *SMAD4*^{KO} NK cells exhibited phosphorylation of SMAD2 and reduced SMAD4 levels (Fig. 6a,b). SB-431542 activity was also validated by the absence of granzyme B and NKG2D downregulation as well as the lack of CD103 acquisition in TGFβ1-treated control cells (Fig. 6c). Despite the effective inhibition of TGFβ signaling, *SMAD4*^{KO} NK cells treated with TGFβ1 showed superior cytotoxicity against HCC116-GFP^{+}Luc^{+} spheroids than control NK cells treated with SB-431542 (Fig. 6d,e). These findings highlight the advantage of preserving SMAD4-independent TGFβ signaling in NK cells to enhance their antitumor function.

SMAD4^{KO} NK cells resist activin A-mediated suppression

SMAD4 is a signaling hub that participates in the transcriptional changes induced by other members of the TGFβ superfamily. Among those, activin A is also produced in the TME and contributes to attenuate NK cell effector function[19,27]. Activin A shares the canonical SMAD2/SMAD3/SMAD4 pathway with TGFβ[28] yet signaling is initiated by specific type II receptors (ActRIIA, ActRIIB) that promiscuously couple to different type I receptors, mainly ActRIB, but also ActRIA and ActRIC[28]. Consequently, activin A could contribute to NK cell inhibition, also in situations of TGFβ or TGFβ-receptor blockade. Analysis of RNA-seq data showed expression of activin A type I and type II receptors in NK cells. Both control and *SMAD4*^{KO} NK cells expressed *ACVR2A* and *ACVR1* at basal conditions, while switching to *ACVR2B* and *ACVR1B* upon TGFβ exposure (Fig. 7a). Treatment with activin A induced a reduction in granzyme B levels, less pronounced than that induced by TGFβ1 (Fig. 7b,c). Nonetheless, while control NK cells demonstrated a reduction in cytotoxicity toward HCT116 cells in response to activin A, *SMAD4*^{KO} NK cells retained their cytotoxic capacity, indicating their resistance to activin A-mediated suppression (Fig. 7d).

SMAD4^{KO} in diverse NK cell products in clinical development

Anti-CD19-CAR-NK cells have demonstrated clinical activity without major toxic effects[2], paving the way for CAR-NK cell therapy development.

https://doi.org/10.1038/s41590-025-02103-z

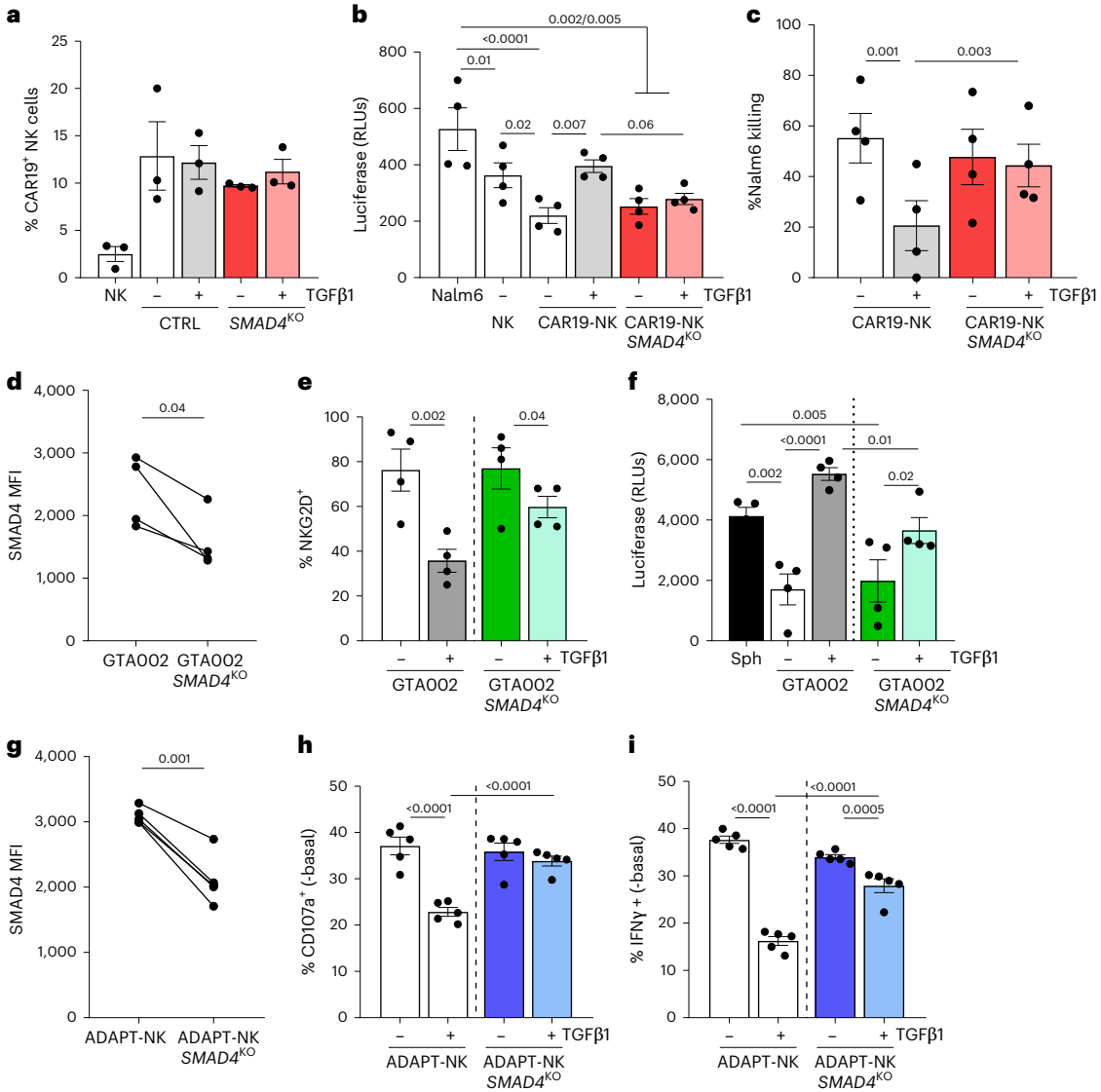

Fig. 8 | The knockout of *SMAD4* improves the resistance to TGFβ of diverse NK cell products in clinical development. a–**c**, Control and *SMAD4*^{KO} NK cells transduced with anti-CD19-CAR lentivirus were cultured with IL-2 ± TGFβ1 for 6 days. **a**, Mean ± s.e.m. percentage of control or *SMAD4*^{KO} NK cells transduced with the anti-CD19-CAR by flow cytometry. Data are from three independent experiments. **b**,**c**, CAR19-transuced control or *SMAD4*^{KO} NK cells treated with IL-2 ± TGFβ1 were cocultured with Nalm6-GFP^{+}-Luc^{+} for 3 h at a 4:1 E:T ratio. **b**, Mean ± s.e.m. luciferase counts at the end of the coculture in the indicated conditions. Dots show data from technical replicates ($n = 4$) in a representative experiment. **c**, Mean ± s.e.m. percentage of Nalm6 cell killing in the indicated conditions. Dots show data of independent experiments with CD19-CAR NK cells from different donors ($n = 4$). **d**–**f**, Control and *SMAD4*^{KO} GTA002 cells were cultured in IL-2 ± TGFβ1 for 5 days. Data are from four independent experiments. GTA002 cells from different cord-blood units are presented as independent dots. **d**, SMAD4 MFI in control and *SMAD4*^{KO} GTA002 cells at day 5. **e**, Mean ± s.e.m. percentage of NKG2D^{+} control or *SMAD4*^{KO} GTA002 cells in the indicated conditions. **f**, Mean luciferase activity remaining after 24 h coculture of HCT116-GFP^{+}-Luc^{+} spheroids with control or *SMAD4*^{KO} GTA002 cells in the indicated conditions. Sph, spheroid. **g**–**i**, Control or *SMAD4*^{KO} ADAPT-NK cells were cultured for 5 days with IL-2 ± TGFβ1. Degranulation and IFNγ production were analyzed by coculturing control or *SMAD4*^{KO} ADAPT-NK cells with K562 cells at a 1:1 E:T ratio for 4 h. Dots represent data from independent experiments using ADAPT-NK cells from different donors. **g**, SMAD4 MFI in control and *SMAD4*^{KO} ADAPT-NK cells at day 5. **h**,**i**, Mean ± s.e.m. percentage of CD107^{+} (**h**) and IFNγ^{+} (**i**) control and *SMAD4*^{KO} ADAPT-NK cells in the indicated conditions. Basal degranulation and IFNγ production in the absence of target were subtracted. Statistical significance was calculated by a two-tailed, paired Student's *t*-test in **d** and **g**, and by one-way ANOVA followed by Fisher's test in **b**, **c**, **e**, **f**, **h** and **i**.

To investigate the impact of *SMAD4*^{KO} on CAR-NK cell function, control and *SMAD4*^{KO} NK cells were transduced with an anti-CD19-CAR construct[29]. As observed in expanded NK cells, knockout of *SMAD4* prevented the downregulation of NKG2D and CD16 while maintaining CD103 induction in CAR19-NK cells treated with TGFβ1 (Extended Data Fig. 9a–c). Cytotoxicity assays against the B cell leukemia cell line Nalm6-GFP^{+}-Luc^{+} revealed that CAR19-NK cells were sensitive to TGFβ1 suppression, even when activated through the CD137 and CD28 signaling domains of the CAR construct (Fig. 8a–c). Notably, knocking out *SMAD4* preserved their cytotoxic function against Nalm6 in the presence of TGFβ1 (Fig. 8a–c).

Alternative NK cell-based platforms in clinical development include cord-blood stem cell-derived NK cell products (that is, GTA002 as developed by Glycostem)[30] and expanded peripheral blood NK cells with adaptive features (that is, ADAPT-NK)[31]. Subsequent experiments evaluated the sensitivity of these NK cell products to TGFβ suppression and whether knockout of *SMAD4* could enhance their antitumor activity. *SMAD4*^{KO} was successfully achieved in both NK cell products (Fig. 8d,g), conferring resistance to NKG2D downregulation by TGFβ1 (Fig. 8e and Extended Data Fig. 9e). Consistent with previous findings, *SMAD4*^{KO} in stem cell-derived NK cells displayed enhanced cytotoxicity

against HCT116 spheroids in the presence of TGFβ1 as compared to their control counterparts (Fig. 8f). Similarly, knocking out *SMAD4* prevented TGFβ1-induced reductions in degranulation and IFNγ production by ADAPT-NK cells against the K562 cell line (Fig. 8h,i), which, in addition, also showed preserved expression of granzyme B and CD16 expression in the presence of TGFβ1 (Extended Data Fig. 9f,g). Of note, knocking out *SMAD4* did not alter the phenotype and function of any of these NK cell products in homeostatic conditions.

Altogether, these results underscore the translational potential of knocking out *SMAD4* for improving NK cell-based immunotherapies.

Discussion

The effectiveness of NK cell adoptive transfer for solid tumors remains a significant clinical challenge, with TGFβ recognized as a major suppressor of NK cell function and proliferation. Our findings reveal that SMAD4 acts as a molecular switch, uncoupling TGFβ inhibitory effects on NK cell antitumor function from its role in promoting tissue homing and residency. Thus, targeting SMAD4 represents a promising avenue for improving NK cell therapies, particularly for solid tumors.

Previous studies in mice showed that *Smad4* deletion in Ncr1-Cre models caused a reduction in mature NK cell numbers leading to defective antiviral and antitumor immunity[13,16,32]. This defect in NK cell maturation was independent of TGFβ signaling, as NK cells with double deletion of *Tgfbr2* and *Smad4* exhibited similar maturation defects[13,16,33], suggesting that other members of the TGFβ superfamily might regulate NK cell differentiation. Indeed, autocrine BMP signaling has been shown to regulate terminal NK cell differentiation in the thymus by promoting CD122 expression and enabling IL-15 responsiveness[34].

In contrast to these findings in mice, knockout of *SMAD4* in mature human NK cells did not alter their maturation status, functional profile or proliferative capacity under homeostatic conditions, but enhanced their resistance to TGFβ suppression. *SMAD4*^{KO} NK cells retained granzyme B expression in basal conditions and after TGFβ exposure, despite the proposed role of SMAD4 in regulating the granzyme B promoter[13,35]. These findings suggest that SMAD4 is critical for NK cell competence during ontogeny but dispensable in mature NK cells. Alternatively, prolonged *SMAD4* abrogation might disrupt additional homeostatic processes, emphasizing the need for further investigation.

NK cell transcriptomic and phenotypic characterization showed minimal effects of *SMAD4*^{KO} in homeostatic conditions, with only 54 genes affected. Under TGFβ exposure, *SMAD4*^{KO} preserved the expression of key transcription factors, adhesion molecules, activating receptors and cytotoxic effectors involved in NK cell function. *SMAD4*^{KO} NK cells also preserved their cytokine-driven proliferation under TGFβ, likely owing to sustained IL-2RA and IL-15RA expression.

Preservation of SMAD4-independent TGFβ signaling enabled the expression of death receptor ligands (TNFSF10 and FASL)[13,16], tissue-residency integrins and chemokine receptors, enhancing *SMAD4*^{KO} NK cell tumor-homing and infiltration. Furthermore, *SMAD4*^{KO} simultaneously alleviated activin A-mediated suppression[19,27], further improving NK cell resilience in the TME. The potential involvement of SMAD4-independent signaling (for example, TIF1γ) in TGFβ-induced tissue residency and homing warrants further investigation.

SMAD4^{KO} NK cells demonstrated superior tumor control as monotherapy and with tumor antigen-specific antibodies that trigger antibody-dependent cellular cytotoxicity. However, their advantage over control cells was model dependent, suggesting that tumor-intrinsic factors, such as differential sensitivity to effector molecules (that is, IFNγ or death receptor ligands), influence *SMAD4*^{KO} NK cell benefit in vivo. Understanding NK cell-resistance mechanisms will help identify predictive biomarkers of clinical efficacy.

A limitation of our study is the inability to distinguish contributions of *SMAD4*$^{+/-}$ versus *SMAD4*$^{-/-}$ NK cells. Findings in *SMAD4*$^{+/-}$ individuals with JPS revealed that one *SMAD4* allele suffices for NK cell differentiation and HCMV responses[36]. Partial resistance to TGFβ suppression in *SMAD4*$^{+/-}$ NK cells suggests that reducing *SMAD4* allelic dose already confers functional benefits. Future studies should explore differences in proliferation, persistence and activation between *SMAD4*$^{+/-}$ and *SMAD4*$^{-/-}$ NK cells, especially in TGFβ-rich environments and during in vivo adoptive transfer.

Recent clinical trials demonstrate the safety of multiplex CRISPR–Cas9 gene editing in T cells for advanced cancer (NCT03399448)[37], paving the way for similar approaches in NK cell therapies. We developed an efficient and safe CRISPR–Cas9 strategy for knocking out *SMAD4* in NK cells, validated through sequencing, flow cytometry and functional assays. Our results also evidenced the translational potential of *SMAD4*^{KO} for overcoming TGFβ suppression and enhancing the antitumor activity of diverse NK cell platforms in early clinical development, including CAR-NK cells. Remarkably, SMAD4^{KO} in cord-blood-derived (GTA002) and adaptive NK cell products (ADAPT-NK) did not alter their basal phenotype or function but conferred TGFβ resistance. This demonstrates that *SMAD4*^{KO} effects were independent of the methodology used for NK cell expansion.

In conclusion, *SMAD4* knockout by CRISPR–Cas9 offers a versatile and safe strategy to overcome TGFβ suppression and enhance next-generation NK cell-based immunotherapy for solid tumors.

Online content

Any methods, additional references, Nature Portfolio reporting summaries, source data, extended data, supplementary information, acknowledgements, peer review information; details of author contributions and competing interests; and statements of data and code availability are available at https://doi.org/10.1038/s41590-025-02103-z.

References

1. Ruggeri, L. et al. Effectiveness of donor natural killer cell alloreactivity in mismatched hematopoietic transplants. *Science* **295**, 2097–2100 (2002).
2. Liu, E. et al. Use of CAR-transduced natural killer cells in CD19-positive lymphoid tumors. *N. Engl. J. Med.* **382**, 545–553 (2020).
3. Jia, L. et al. Sintilimab plus autologous NK cells as second-line treatment for advanced non-small-cell lung cancer previous treated with platinum-containing chemotherapy. *Front. Immunol.* **13**, 1074906 (2022).
4. Bae, W. K. et al. A phase I study of locoregional high-dose autologous natural killer cell therapy with hepatic arterial infusion chemotherapy in patients with locally advanced hepatocellular carcinoma. *Front. Immunol.* **13**, 879452 (2022).
5. Khatua, S. et al. Phase I study of intraventricular infusions of autologous ex vivo expanded NK cells in children with recurrent medulloblastoma and ependymoma. *Neuro Oncol.* **22**, 1214–1225 (2020).
6. Tauriello, D. V. F. et al. TGFβ drives immune evasion in genetically reconstituted colon cancer metastasis. *Nature* **554**, 538–543 (2018).
7. Cabo, M. et al. CD137 costimulation counteracts TGFβ inhibition of NK-cell antitumor function. *Cancer Immunol. Res.* **9**, 1476–1490 (2021).
8. Batlle, E. & Massagué, J. Transforming growth factor-β signaling in immunity and cancer. *Immunity* **50**, 924–940 (2019).
9. He, W. et al. Hematopoiesis controlled by distinct TIF1gamma and Smad4 branches of the TGFβ pathway. *Cell* **125**, 929–941 (2006).
10. Descargues, P. et al. IKKalpha is a critical coregulator of a Smad4-independent TGFβ-Smad2/3 signaling pathway that controls keratinocyte differentiation. *Proc. Natl Acad. Sci. USA* **105**, 2487–2492 (2008).
11. Derynck, R. & Zhang, Y. E. Smad-dependent and Smad-independent pathways in TGF-β family signalling. *Nature* **425**, 577–584 (2003).

12. Yu, J. et al. Pro- and antiinflammatory cytokine signaling: reciprocal antagonism regulates interferon-gamma production by human natural killer cells. *Immunity* **24**, 575–590 (2006).
13. Wang, Y. et al. SMAD4 promotes TGF-β-independent NK cell homeostasis and maturation and antitumor immunity. *J. Clin. Invest.* **128**, 5123–5136 (2018).
14. Trotta, R. et al. TGF-beta utilizes SMAD3 to inhibit CD16-mediated IFN-gamma production and antibody-dependent cellular cytotoxicity in human NK cells. *J. Immunol.* **181**, 3784–3792 (2008).
15. Gao, Y. et al. Tumor immunoevasion by the conversion of effector NK cells into type 1 innate lymphoid cells. *Nat. Immunol.* **18**, 1004–1015 (2017).
16. Cortez, V. S. et al. SMAD4 impedes the conversion of NK cells into ILC1-like cells by curtailing non-canonical TGF-β signaling. *Nat. Immunol.* **18**, 995–1003 (2017).
17. Castriconi, R. et al. Transforming growth factor beta 1 inhibits expression of NKp30 and NKG2D receptors: consequences for the NK-mediated killing of dendritic cells. *Proc. Natl Acad. Sci. USA* **100**, 4120–4125 (2003).
18. Massagué, J. TGFβ signalling in context. *Nat. Rev. Mol. Cell Biol.* **13**, 616–630 (2012).
19. Rautela, J. et al. Therapeutic blockade of activin-A improves NK cell function and antitumor immunity. *Sci. Signal.* **12**, eaat7527 (2019).
20. Tauriello, D. V. F., Sancho, E. & Batlle, E. Overcoming TGFβ-mediated immune evasion in cancer. *Nat. Rev. Cancer* **22**, 25–44 (2022).
21. Derynck, R., Turley, S. J. & Akhurst, R. J. TGFβ biology in cancer progression and immunotherapy. *Nat. Rev. Clin. Oncol.* **18**, 9–34 (2021).
22. Shaim, H. et al. Targeting the αv integrin/TGF-β axis improves natural killer cell function against glioblastoma stem cells. *J. Clin. Invest.* **131**, 142116 (2021).
23. Yvon, E. S. et al. Cord blood natural killer cells expressing a dominant negative TGF-β receptor: implications for adoptive immunotherapy for glioblastoma. *Cytotherapy* **19**, 408–418 (2017).
24. Healy, L. P. et al. Loss-of-function in SMAD4 might not be critical for human natural killer cell responsiveness to TGF-β. *Front. Immunol.* **10**, 904 (2019).
25. Corsi, G. I., Gadekar, V. P., Gorodkin, J. & Seemann, S. E. CRISPRroots: on- and off-target assessment of RNA-seq data in CRISPR-Cas9 edited cells. *Nucleic Acids Res.* **50**, e20 (2022).
26. Inman, G. J. et al. SB-431542 is a potent and specific inhibitor of transforming growth factor-beta superfamily type I activin receptor-like kinase (ALK) receptors ALK4, ALK5, and ALK7. *Mol. Pharmacol.* **62**, 65–74 (2002).
27. Robson, N. C. et al. Activin-A attenuates several human natural killer cell functions. *Blood* **113**, 3218–3225 (2009).
28. Morianos, I., Papadopoulou, G., Semitekolou, M. & Xanthou, G. Activin-A in the regulation of immunity in health and disease. *J Autoimmun.* **104**, 102314 (2019).
29. Castella, M. et al. Development of a novel anti-CD19 chimeric antigen receptor: a paradigm for an affordable CAR T cell production at academic institutions. *Mol. Ther. Methods Clin. Dev.* **12**, 134–144 (2019).
30. van Vliet, A. et al. Bulk and single-cell transcriptomics identify gene signatures of stem cell-derived NK cell donors with superior cytolytic activity. *Mol. Ther. Oncol.* **32**, 200870 (2024).
31. Haroun-Izquierdo, A. et al. Adaptive single-KIR$^+$NKG2C$^+$ NK cells expanded from select superdonors show potent missing-self reactivity and efficiently control HLA-mismatched acute myeloid leukemia. *J. Immunother. Cancer* **10**, e005577 (2022).
32. Huang, Y.-W. et al. Black raspberries suppress colorectal cancer by enhancing Smad4 expression in colonic epithelium and natural killer cells. *Front. Immunol.* **11**, 570683 (2020).
33. Viel, S. et al. TGF-β inhibits the activation and functions of NK cells by repressing the mTOR pathway. *Sci. Signal.* **9**, ra19 (2016).
34. Hidalgo, L. et al. Expression of BMPRIA on human thymic NK cell precursors: role of BMP signaling in intrathymic NK cell development. *Blood* **119**, 1861–1871 (2012).
35. Liu, X. et al. SMAD4, activated by the TCR-triggered MEK/ERK signaling pathway, critically regulates CD8$^+$ T cell cytotoxic function. *Sci. Adv.* **8**, eabo4577 (2022).
36. López-Botet, M., De Maria, A., Muntasell, A., Della Chiesa, M. & Vilches, C. Adaptive NK cell response to human cytomegalovirus: facts and open issues. *Semin. Immunol.* **65**, 101706 (2023).
37. Stadtmauer, E. A. et al. CRISPR-engineered T cells in patients with refractory cancer. *Science* **367**, eaba7365 (2020).

[1]University Pompeu Fabra (UPF), Barcelona, Spain. [2]Hospital del Mar Research Institute (IMIM), Barcelona, Spain. [3]Institut de Biotecnologia i Biomedicina, Cell Biology, Physiology and Immunology Deptartments, Universitat Autònoma de Barcelona, Bellaterra, Spain. [4]Precision Immunotherapy Alliance, The University of Oslo, Oslo, Norway. [5]Department of Cancer Immunology, Institute for Cancer Research Oslo, Oslo University Hospital, Oslo, Norway. [6]Department of Immunology, Hospital Clínic de Barcelona (HCB), Institut d'Investigacions Biomèdiques August Pi i Sunyer (IDIBAPS), Joint Platform of Immunotherapy Hospital Sant Joan de Deu – HCB, University of Barcelona, Barcelona, Spain. [7]Department of Pathology and Immunology, Washington University School of Medicine, St. Louis, MO, USA. [8]Glycostem Therapeutics, Oss, the Netherlands. [9]Department of Gastroenterology, Hospital Clínic de Barcelona, Institut d'Investigacions Biomèdiques August Pi i Sunyer (IDIBAPS), Centro de Investigación Biomédica en Red de Enfermedades Hepáticas y Digestivas (CIBERehd), University of Barcelona, Barcelona, Spain. [10]IIS Aragon Foundation/ Dpt. Microbiology, Radiology Pediatry and Public Health, University of Zaragoza, Centro de Investigación Biomédica en Red de Enfermedades Infecciosas (CIBERinfec), Zaragoza, Spain. [11]Centro de Investigación Biomédica en Red de Cáncer (CIBERONC), Madrid, Spain. [12]Department of Oncology, Hospital del Mar, Barcelona, Spain. [13]Miltenyi Biotec B.V. & Co. KG, Bergisch Gladbach, Germany. [14]Center for Infectious Medicine, Department of Medicine Huddinge, Karolinska Institutet, Stockholm, Sweden. [15]Institució Catalana de Recerca i Estudis Avançats, ICREA, Barcelona, Spain. ✉e-mail: aura.muntasell@uab.cat

Methods

Human samples

PBMCs were obtained from healthy adult volunteers and two individuals with JPS by Ficoll-Hypaque density-gradient centrifugation (Lymphoprep). Cells were cultured overnight in complete RPMI 1640 GlutaMAX (Gibco) medium (100 U ml^{-1} and 100 µg ml^{-1} penicillin and streptomycin, respectively, Invitrogen; 1 mM sodium pyruvate, Gibco; 10% FBS, Gibco) supplemented with recombinant IL-2 (200 U ml^{-1}, Proleukin). Detailed participant information is provided in Supplementary Methods.

Cell lines

HCT116 colorectal carcinoma cells and their GFP-luciferase-expressing derivative line (HCT-GFP$^+$Luc$^+$) were cultured in DMEM (Sigma-Aldrich) supplemented with penicillin and streptomycin (100 U ml^{-1} and 100 µg ml^{-1}, respectively, Invitrogen), sodium pyruvate (1 mM, Gibco) and 10% FBS (Gibco). The B lymphoblastoid cell line 8866, the HLA class-I-negative human erythroleukemic cell lines K562, K562-HLA-E^{hi} and K562 engineered to express 41BB ligand and membrane-bound IL-15 and IL-21, the HCC1954, a HER2-positive breast carcinoma cell line, and its derivative HCC1954-GFP$^+$Luc$^+$, and Nalm6-GFP$^+$Luc$^+$ cells were maintained in RPMI 1640 GlutaMAX supplemented with penicillin and streptomycin (100 U ml^{-1} and 100 µg ml^{-1}, respectively, Invitrogen), sodium pyruvate (1 mM, Gibco) and 10% FBS (Gibco). The K562 (CRL-3344), HCT116 (CCL247EMT) and HCC1954 (CRL-2338) cell lines were purchased from the American Type Culture Collection (ATCC), the 8866 B-LCL and Nalm6-GFP$^+$-Luc$^+$ cells were kindly provided by M. López-Botet (Universitat Pompeu Fabra) and M. Juan (Hospital Clínic de Barcelona), respectively. HCT116-GFP$^+$-Luc$^+$ cells were kindly provided by J. Pardo (Universidad de Zaragoza). The K562-CD137L-IL15tmb-IL21tmb cells were kindly provided by W. S. Wels (Georg-Speyer-Haus). The K562-HLA-E^{high} cells were generated by overexpressing HLA-E*0.1:0.1 as a single-chain construct covalently linked to b2m and to the HLA-G sequence peptide VMAPRTLFL (Gsp) at the Institute for Cancer Research Oslo. HCC1954-GFP$^+$-Luc$^+$ cells were generated by lentiviral transduction using the plasmid pHIV-Luc-ZsGreen (Addgene, 39196).

CRISPR–Cas9 gene editing of *SMAD4* in expanded NK cells

PBMCs from healthy donors were cocultured with irradiated 8866 cells (40 Gy) at a 3:1 ratio in complete RPMI 1640 GlutaMAX (Gibco). At day 7, NK cells were isolated by negative selection using an NK cell isolation kit (Miltenyi Biotec), following the manufacturer's protocol, achieving >99% purity (mean ± s.d. 99.79% ± 0.13%) with minimal T cell contamination (0.19% ± 0.15%). No B cells or myeloid cells were detected. CRISPR–Cas9 editing of *SMAD4* was done using gRNA targeting exon 5 (crRNA: GTCGATGCACGATTACTTGG) designed by CRISPRscan[38] and synthesized by IDT. The gRNAs (crRNA and a fluorescently labeled tracrRNA-ATTO550) were prepared by incubation at a 1:1 molar ratio at 95 °C for 5 min. Cas9–gRNA RNPs were prepared by combining Cas9 enzyme (IDT) and the prepared single guide RNA at a 1:3 molar ratio for 20 min at room temperature. NK cells were electroporated with pre-assembled Cas9–gRNA RNP complexes using a Neon Transfection System (1,900 V, 20 ms, 1 pulse). After electroporation, cells were cultured in complete RPMI 1640 with with IL-2 (200 U ml^{-1}) ± TGFβ1 (5 ng ml^{-1}) for 6 days before use or cryopreservation. In some experiments, nucleofected NK cells were treated with IL-2 and activin A (100 ng ml^{-1}) or with the TGFβRI inhibitor SB-431542 (20 µM, Sigma-Aldrich) and TGFβ1 (5 ng ml^{-1}). SB-431542 was added before TGFβ1 and refreshed daily along the culture. Nucleofection efficiency was assessed 24 h after electroporation by Fortessa flow cytometer (BD Biosciences).

Generation and CRISPR–Cas9 engineering of stem cell-derived GTA002 NK cells

Fresh and frozen umbilical cord-blood units were purchased from A. Nolan (United Kingdom) or NHS Blood and Transplant (United Kingdom), and mononuclear cells were isolated by Ficoll Paque Plus (1.077 g ml^{-1}, GE Healthcare) density-gradient centrifugation. Hematopoietic CD34$^+$ stem cells were selected from the mononuclear cells using the CD34$^+$ magnetic microbead kit (Miltenyi Biotech) according to the manufacturer's protocol. CD34$^+$ cells were seeded in six-well tissue culture-treated plates (Corning) for expansion culture in Glycostem Basal Growth Medium (Fertipro) supplemented with human serum (Sanquin), thrombopoietin, IL-7, FMS-like tyrosine kinase 3 ligand (Flt-3L), granulocyte–macrophage colony-stimulating factor, IL-6, stem cell factor (all from Cellgenix) and Neupogen (G-CSF, Amgen), as described previously[30]. After 9 days, thrombopoietin was replaced by IL-15 (Cellgenix) and, after 14 days of NK progenitor expansion, Flt-3L was replaced by Proleukin (IL-2, Novartis) for the NK cell differentiation phase. GTA002 NK cells were cryopreserved at the end of the culture. Thawed GTA002 NK cells were cultured in NK-MACS-supplemented 10% AB sera, IL-2 (1,000 U ml^{-1}) and IL-15 (20 ng ml^{-1}). Seven days after thawing, cells were nucleofected with SMAD4-targeting Cas9–gRNA RNP, as described above, and further cultured for 5 days in NK-MACS media with IL-2 (200 U ml^{-1}) ± rTGFβ1 (5 ng ml^{-1}) before phenotypic and functional assays.

Expansion and engineering of ADAPT-NK cells

For the expansion and generation of ADAPT-NK cells CD3/CD19-depleted PBMCs were cocultured with 100-Gy- or 200-Gy-irradiated K562 feeder cells transfected with lentiviral construct to express high levels of HLA-E with an HLA-G-leader-derived peptide at a 1:2 ratio in G-Rex24 plates (Wilson Wolf) at 0.5 × 10^6 total cells per cm^2. Cells were cultured in GMP-grade Stem Cell Growth Medium (CellGenix) supplemented with 10% human AB serum (TCS Biosciences or Access Biologicals), 2 mM L-glutamine (Cytiva, Fisher Scientific) and 100 IU ml^{-1} human recombinant IL-2 (Proleukin) for 11 days with 60% medium exchange on day 7, and IL-2 addition days 4, 7 and 10, as previously described[31]. ADAPT-NK cells were nucleofected with the same gRNA targeting SMAD4 exon 5 using Amaxa 4D (Lonza), program CM-137, and further cultured for 5 days in IL-2 (200 U ml^{-1}) ± rTNF-β (5 ng ml^{-1}) before phenotypic and functional assays.

NK cell immunophenotyping by multiparametric flow cytometry

NK cells were incubated with aggregated human IgG (10 µg ml^{-1}) for Fc blocking. In indirect staining, cells were incubated with hybridoma supernatants (that is, KIRmix), washed and subsequently incubated with the corresponding secondary antibody followed by incubation with combinations of directly labeled antibodies for extracellular markers. For intracellular staining, cells were fixed and permeabilized (fixation/permeabilization kit, BD Biosciences) and stained for intracellular antigens. All incubations were done for 20 min on ice. In non-fixed samples, DAPI (1 µg ml^{-1}, Sigma-Aldrich) was added before data acquisition as a viability dye. For SMAD4 staining, NK cells were fixed and permeabilized with Invitrogen eBioscience Foxp3/Transcription Factor Staining Buffer Set (Thermo Fisher) and subsequently incubated with anti-SMAD4 (Cell Signaling) for 1 h at room temperature followed by an incubation with a polyclonal donkey anti-rabbit IgG Alexa Fluor 488. Data were acquired on Fortessa or LSR II flow cytometers (BD Biosciences) and analyzed with FlowJo X software (v10.8.1). All antibodies used for flow cytometry are listed in Supplementary Table 1.

Functional assays for NK cell activity

NK cell degranulation was assessed by monitoring CD107a mobilization following a 4-h coculture with K562 cells at a 1:1 E:T ratio, including the anti-CD107a-FITC (clone H4A3, BD Biosciences) and monensin (5 µg ml^{-1}, Sigma-Aldrich). When indicated, TNF (infliximab-CF Blue) was also analyzed by intracellular staining at the end of the coculture. The anti-IFNγ-APC (clone B27, BD Biosciences) was used for intracellular staining in ADAPT-NK assays. For cytotoxicity assays, NK cells were

cultured with HCT116 cells at the indicated E:T ratios for 2 h or 4 h. Activated caspase-3 in HCT116 was analyzed by intracellular staining and flow cytometry. HCT116 cells were gated based on forward and size scatter (FSC/SSC) and by CD45 exclusion. Basal levels of active caspase-3 were subtracted in each other condition.

Production of CCL5, TNF and IFNγ was measured after 2 h coculture with HCT116 cells and analyzed by ELISA using DY278, DY210 (R&D Systems) and 88-7316-88 (Invitrogen), following the manufacturer's instructions.

For spheroid formation 5,000 HCT116-GFP$^+$-Luc$^+$ cells of HCC1954-GFP$^+$-Luc$^+$ cells were seeded in ultralow attachment 96-well plates (Costar), centrifuged at 1,000*g* for 10 min and cultured for 72 h. Control NK and *SMAD4*^{KO} NK cells (100,000 cells), treated or not with TGFβ1, were cocultured with spheroids. The remaining luciferase activity at 24 h, proportional to Luc$^+$ alive cells, was measured by incubating with luciferin substrate (10 µg ml^{-1}, Sigma) for 5 min. Luminescence was measured using an FB12 Tube Luminometer or an Orion II Microplate Luminometer (Berthold Technologies). In some experiments, NK cells were labeled with PKH26 dye (Sigma-Aldrich), following the manufacturer's instructions, before coculture with HCT116 spheroids. Images were acquired at 6, 24 and 30 h using a Zeiss Cell Observer HS microscope with *z*-stacks (13.5 µm, total magnification ×5) in the green (HCT116, GFP), red (NK, PKH26) and transmitted light channels. Each condition was tested in five replicates. GFP integrated density was quantified using ImageJ (v.54a).

In vivo xenograft models

All animal experiments were conducted in compliance with protocols approved by the Barcelona Biomedical Research Park Animal Facility and Generalitat de Catalunya Animal Care and Use Committee (EARA-20-0045). Eight-week-old NOD/Scid/γc$^{-/-}$ (NSG) female mice (Jackson Laboratory, strain 005557) were used for in vivo studies. Tumors were established by subcutaneous injection of HCC1954 human breast cancer cells (4×10^5) or HCT116 colorectal cancer cells (2.5×10^6) embedded in Matrigel into the right flank. Tumor volume was calculated using the formula (width^2 × length × π)/6. When tumors reached 100 mm^3, mice were randomized into groups (n = 5/6 per condition) and treated with one of the following regimens: HCC1954 xenografts: (i) anti-HER2 antibodies (trastuzumab and pertuzumab (1 mg per kg body weight, each)); (ii) control NK cells (0.2×10^6 cells); (iii) *SMAD4*^{KO} NK cells (0.2×10^6 cells); (iv) control NK cells (0.1×10^6 cells) in combination with trastuzumab/pertuzumab (1 mg per kg body weight, each); and (v) *SMAD4*^{KO} NK cells (0.1×10^6 cells) in combination with trastuzumab/pertuzumab (1 mg per kg body weight, each). Antibodies were administered intraperitoneally every 3–4 days. NK cells were injected intratumorally once a week for 3 weeks, along with recombinant human IL-2 (rhIL-2, 200 IU per mouse) and sustained by intraperitoneal rhIL-2 (20,000 IU per mouse) every 3–4 days. Mice bearing HCT116 xenografts only received the described NK cell treatment and IL-2 support. Mice were euthanized when developing signs of discomfort per the protocol and as recommended by a veterinarian, and a maximal tumor size of 1,500 mm^3 was not exceeded.

Anti-CD19-CAR-NK cells generation and cytotoxicity assay

CD19-CAR NK cells were generated at the Immunotherapy Department of Hospital Clínic-IDIBAPS, Barcelona, as previously described[29,39]. Control and *SMAD4*^{KO} NK cells were restimulated by coculture with irradiated (40 Gy) K562-CD137L-IL15tmb-IL21tmb cells at a 1:1 ratio. On day 7, NK cells were transduced with lentivirus supernatants (multiplicity of infection of 20) with 6 µg ml^{-1} polybrene, followed by centrifugation at 2,000 rpm for 1 h at 37 °C. After 24 h, cells were cultured in NK-MACS medium (Miltenyi Biotec) with IL-2 (200 U ml^{-1}) ± TGFβ1 (5 ng ml^{-1}) for 6 days. CD19-CAR expression was monitored with the CD19-CAR detection reagent-biotin (Miltenyi Biotec) by flow cytometry. CD19-CAR control or *SMAD4*^{KO} NK cells were cocultured with Nalm6-Luc-GFP at a 4:1 E:T ratio for 3 h. Residual luciferase activity, reflecting viable target cells, was assessed by incubation with luciferin substrate (10 µg ml^{-1}, Sigma) for 5 min, followed by luminescence measurement using an FB12 Tube Luminometer (Berthold Technologies).

Spheroid penetrance analysis by light-sheet imaging with UltraMicroscope Blaze

Control NK and *SMAD4*^{KO} NK cells were cocultured with HCT116 spheroids for 1 h. Spheroid processing was done according to Miltenyi Biotec's instructions for 'Immunostaining and clearing of stem cell-derived cerebral organoids for three-dimensional imaging analysis'[40]. Fixed spheroids were stained with anti-CD45-Vio R667 (10 µg ml^{-1}, Miltenyi Biotec), anti-Epcam-Alexa Fluor 488 (5 µg ml^{-1}, Abcam) and propidium iodide (PI, 0.2 µg ml^{-1}, Miltenyi Biotec). Specimens were treated using tissue Clearing Kit and Imaging Solution (Miltenyi Biotec) and were scanned with the UltraMicroscope Blaze (Miltenyi Biotec). Samples were scanned using an objective lens at ×12 magnification with 150 ms of exposure and a 2-µm step size in the transverse plane. Three-dimensional spheroid reconstruction was done using ImageJ (v54a) and the distance between the spheroid surface and each NK cell was analyzed with Imaris software (10.0), as previously described[41].

NK cell proliferation assays

Control or *SMAD4*^{KO} NK cells were labeled with 0.5 µM CFSE (CellTrace CFSE Cell Proliferation Kit, Invitrogen) before culturing in plates coated with anti-NKp46 (clone BAB281, 5 µg ml^{-1}) in the presence of rIL-2 (200 U ml^{-1}) ± TGFβ1 (5 ng ml^{-1}). After 5 days, CFSE fluorescence was analyzed by flow cytometry and expressed as the percentage of divided cells. Alternatively, thawed control or *SMAD4*^{KO} NK cells were cultured with irradiated (40 Gy) K562-CD137L-IL15tmb-IL21tmb cells at a 1:1 ratio for 7 days, and restimulated with feeder cells in the presence of rIL-2 (200 U ml^{-1}) ± rTGFβ1 (5 ng ml^{-1}) for 7 more days. NK cell expansion from day 7–14 was quantified by cell counting in a Neubauer chamber. For assessing long-term stability, control and *SMAD4*^{KO} NK cells previously generated and cryopreserved at day 14 were thawed and restimulated with K562-CD137L-IL15tmb-IL21tmb at 1:1 ratio for two consecutive weeks.

NK cell migration assay

Control or *SMAD4*^{KO} NK cells (50,000) pretreated with IL-2 (200 U ml^{-1}) and TGFβ1 (5 ng ml^{-1}) were placed in the upper chamber of a 96-well Transwell plate (5-µm pore size; Corning). Serum-free medium containing CCL5, CXCL9, CXCL10 (50 ng ml^{-1}; PeproTech) or CXCL12 (SDF-1, 100 ng ml^{-1}; R&D) was placed in the lower chamber. Plates were incubated for 2 h at 37 °C, and the number of cells that migrated was determined by automated counting in a 70-µl aliquot using an LSR II flow cytometer. Migration was expressed as a percentage of total input cells.

Western blot of TGFβ signaling mediators

PBMC, NK, HCT116 or HT29 cell pellets were lysed in RIPA buffer, supplemented with protease and phosphatase inhibitors (10 mM β-glycerol-phosphate, 2 mM Na_3VO_4, 5 mM NaF and 1 mM protease inhibitor cocktail; P8340, Sigma-Aldrich) for 20 min on ice. Protein extracts were resolved by SDS–PAGE on 10% polyacrylamide gels and transferred onto PVDF membranes (Immobilon, Millipore). Membranes were blocked in 5% milk or 10% bovine serum albumin in Tris-buffered saline with 0.05% Tween 20 (TBST) for 1 h and incubated overnight at 4 °C with primary antibodies. The following primary antibodies were used: anti-Smad4 (46535, Cell Signaling; 1:1,000 dilution), anti-Smad7 (MAB2029, R&D Systems; 1:1,000 dilution), anti-Phospho-Smad2 (Ser465/467, 138D4, Cell Signaling; 1:1,000 dilution), anti-TGFβRII (sc-17791, Santa Cruz Biotechnology; 1:100 dilution), anti-TIF1γ (A301-060A, Bethyl Laboratories; 1:1,000 dilution) and anti-β-actin (A5441, Sigma-Aldrich). Membranes were washed in TBST and incubated for 1 h at room temperature with horseradish peroxidase-conjugated secondary antibodies (anti-rabbit or anti-mouse; GE Healthcare, 1:2,500 dilution except for β-actin 1:20,000 dilution). Signal was developed

with ECL substrate (SuperSignal West Pico or Femto Chemiluminescent Substrate, Thermo Fisher) and band integrated density was quantified using ImageJ (v54a).

Analysis of publicly available microarray data of NK cells treated or not with TGFβ

The effects of TGFβ on the transcriptome of CD16-activated NK cells have been previously characterized[7] and are available as part of the GSE156200 SuperSeries. Genes differentially expressed between α-CD16-activated NK cells ± TGFβ1-treated (|log fold change| > 0.5 and *P* value < 0.05) were analyzed using Metascape (3.1.3)[42], for biological functions, pathways and networks modulated by TGFβ in activated NK cells.

Transcriptomic characterization of *SMAD4*^{KO} primary NK cells by RNA-seq

RNA-seq sample processing and analysis were conducted by Pompeu Fabra University Genomic Core Facility, Barcelona. GSEA was performed by Mar Genomics Facility at IMIM, Barcelona. Total RNA was extracted from control NK and *SMAD4*^{KO} NK cells treated or not with TGFβ1, from three independent donors (RNeasy Micro Kit, 74004, Qiagen). Next-generation sequencing libraries were prepared with the NebNext Ultra II Directional RNA Library Prep Kit for Illumina (New England BioLabs) using 500 ng of RNA per sample, with Poly(A) capture. Quality and concentration were assessed with TapeStation D1000 (Agilent Technologies). Libraries were pooled in equimolar proportions, amplified by qPCR with specific primers and sequenced in a NextSeq High Output 2 × 75-cycle run (Illumina). Reads were mapped with STAR (version 2.5.9a) against the human reference from Ensembl (version GRCh38), and counts were obtained with HTSeq (version 0.9.1). MultiQC (version 1.9) was used for quality-control assessment. DESeq2 and limma R packages (version 4.0.0) were used for the analysis of DEGs. Genes with a *P* value < 0.05 and |log fold change|> 4 were considered significantly different between conditions. DEGs between control and *SMAD4*^{KO} NK cells treated with TGFβ1 were loaded into the Metascape software (3.1.3)[42] to analyze the biological functions, pathways and networks modulated by SMAD4. GSEA was performed using the R package 'clusterProfiler' (version 4.0.0)[43] against gene sets derived from GSE78897 (ref. 44). CRISPRroots tool (v1.2) was used for off-target assessment in CRISPR–Cas9-edited cells[25].

Analysis of *SMAD4* allelic variants and putative off-targets in engineered NK cells

Targeted analysis of SMAD4 exon 5 and potential off-target loci (*CREBBP*, *DCTN5* and *NUFIP2*) was performed in control NK and *SMAD4*^{KO} NK cells treated or not with TGFβ1. A two-step PCR protocol was used for amplification: (i) gene-specific primers including overhangs compatible with NEB universal primers (listed in Supplementary Table 2) were used for initial amplification with KAPA HiFi HotStart Ready Mix (Roche). PCR conditions: initial denaturation for 3 min at 95 °C, followed by 25 cycles of 98 °C for 20 s, 60 °C for 15 s, 72 °C for 20 s and a final elongation for 1 min at 72 °C. (ii) Barcodes were introduced using Illumina universal primers and indexed primers (NEB, E7335S) under the following conditions: initial denaturation for 3 min at 95 °C followed by 8 cycles of 98 °C for 20 s, 60 °C for 15 s, 72 °C for 20 s and a final elongation for 1 min at 72 °C. PCR products were purified by QIAquick PCR Purification Kit (Qiagen) and sequenced on an Illumina miSeq platform. Reads were aligned to the target region in the human genome (hg38), and data were analyzed by the CRISPR-Analytics platform[45] (https://synbio.upf.edu/crispr-a/), which runs the nextflow pipeline (https://bitbucket.org/synbiolab/crispr-a_nextflow/).

Statistical analysis

Statistics were calculated using GraphPad Prism (v8.0) or in R base and R package edgeR (v 3.22.3). Statistical methods are given in the figure legends.

Ethics and inclusion statement

Experiments involving expansion of ADAPT-NK from healthy donors were approved by the regional ethics committee in Norway (Regional etisk komité (REK): 2018/2482), experiments involving expansion of NK cells from healthy donors were approved by the Clinical Research Ethics Committee, Parc de Salut Mar (no. 2018/787/I). Studies on individuals with JPS were approved by the Clinical Research Ethics Committee at Hospital Clínic de Barcelona (no. HCB/2020/0290). Written informed consent was obtained from all participants and the study adhered to the Declaration of Helsinki.

Reporting summary

Further information on research design is available in the Nature Portfolio Reporting Summary linked to this article.

Data availability

Processed bulk RNA-seq data are available through the Gene Expression Omnibus under accession number GSE248292. Raw data on SMAD4 exon 5 amplimers and putative off-target gene sequences are available at the European Nucleotide Archive under accession number PRJEB70283. The K562-CD137L-IL15tmb-IL21tmb cell line was provided under a material transfer agreement between Georg-Speyer-Haus and St. Jude Children's Research Hospital with IMIM-Hospital del Mar Medical Research Institute. GTA002 cells were provided under a material transfer agreement between Glycostem and IMIM-Hospital del Mar Medical Research Institute. All other data needed to evaluate the conclusions in the paper are present in the paper or Supplementary Information. Source data are provided with this paper.

References

38. Moreno-Mateos, M. A. et al. CRISPRscan: designing highly efficient sgRNAs for CRISPR-Cas9 targeting in vivo. *Nat. Methods* **12**, 982–988 (2015).
39. Herrera, L. et al. Adult peripheral blood and umbilical cord blood NK cells are good sources for effective CAR therapy against CD19 positive leukemic cells. *Sci. Rep.* **9**, 18729 (2019).
40. Gregorius, J. et al. Small extracellular vesicles obtained from hypoxic mesenchymal stromal cells have unique characteristics that promote cerebral angiogenesis, brain remodeling and neurological recovery after focal cerebral ischemia in mice. *Basic Res. Cardiol.* **116**, 40 (2021).
41. Ryder, P. V. & Lerit, D. A. Quantitative analysis of subcellular distributions with an open-source, object-based tool. *Biol. Open* **9**, bio055228 (2020).
42. Zhou, Y. et al. Metascape provides a biologist-oriented resource for the analysis of systems-level datasets. *Nat. Commun.* **10**, 1523 (2019).
43. Yu, G., Wang, L.-G., Han, Y. & He, Q.-Y. clusterProfiler: an R package for comparing biological themes among gene clusters. *OMICS* **16**, 284–287 (2012).
44. Koues, O. I. et al. Distinct gene regulatory pathways for human innate versus adaptive lymphoid cells. *Cell* **165**, 1134–1146 (2016).
45. Sanvicente-García, M. et al. CRISPR-Analytics (CRISPR-A): a platform for precise analytics and simulations for gene editing. *PLoS Comput. Biol.* **19**, e1011137 (2023).

Acknowledgements

We are grateful to W. S. Wels (Georg-Speyer-Haus) for providing the K562-CD137L-IL15tmb-IL21tmb cell line, M. Otero and T. Ocaña for collaboration in obtaining blood samples, O. Fornas for advice on flow cytometry, J. Pereira, M. Tormo and N. Bonet for microarray and RNA-seq data analysis, and to volunteer blood donors and individuals with JPS for their participation in the study. We thank E. Sohlberg and M. T. Wiiger for advice and culture of the ADAPT-NK product. We acknowledge the support from Carrera de la mujer de Monzon

and ASPANOA (Association of Parents of Children with Cancer of Aragon). We are grateful to A. Moretta (University of Genoa) for the anti-NKG2A antibody (z199), to L. Lanier (University of California) for the anti-KIR3DL1 antibody (DX9), to S. Ferrini (University of Genoa) for the anti-KIR2DL2/S2/L3 antibody (C.H.-L.), to F. Sánchez-Madrid (Hospital Universitario la Princesa, Madrid) for the anti-CD18 antibody (TS1/18) and to J. E. de Vries (The Netherlands Cancer Institute) for the anti-CD3 antibody (SPV.T3b). This work was supported by grants PI19/00328 and PI22/00040 (to A.M.), ICI24/00041 (to A.M. and C.M.), PI21/00002 (to J.A.) funded by Instituto de Salud Carlos III (ISCIII) and co-funded by the European Union, Generalitat de Catalunya SGR863 (to M.L.-B. and A.M.), 2024PROD00086 (to A.M.), EC Horizon 2020 Marie Sklodowska Curie-Innovative Training Network 765104 (to A. Rea, M.L.-B., N.M., K.-J.M. and J.S.), Ministerio de Ciencia, Innovación y Universidades/FEDER CNS2023-144487 (to A.M.), CIBERONC: CB16/12/00241 (to J.A.), PID2020-113963RBI00 (to J.P.), PID2023-147310OB-I00 (to T.C.-T.), Gobierno de Aragón B29-23R (to J.P.), AECC postdoctoral fellowship POSTD234709BLAS (to S.B.-B.), Research Council of Norway 275469 and 237579 (to K.-J.M.), the Research Council of Norway through its Centres of Excellence scheme 332727 (to K.-J.M.), the Norwegian Cancer Society-190386, 223310 (to K.-J.M.), The South-Eastern Norway Regional Health Authority 2021-073 and 2024-053 (to K.-J.M.), Knut and Alice Wallenberg Foundation 2018.0106 (to K.-J.M.), Swedish Foundation for Strategic Research (to K.-J.M.) and the US National Cancer Institute P01 CA111412, P009500901 (to K.-J.M.) and CRIS EXCELLENCE 19–30, funded by CRIS Contra el Cáncer (to C.M.).

Author contributions

A.M. conceived and designed the project. A. Rea, S.S.-H., J.S., J.V., B.B., M.S.-G., M.C., E.L., M.Q., F.Q., S.B.-B., L.P. and E.A.-P. performed experiments and/or data analyses. A.M. and M.L.-B. supervised the research. A.M., M.L.-B., M.G., J.A., T.C.-T., A. Rovira and C.M. acquired funding. F.B. and M.J. provided access to JPS samples. N.M. and C.Z. helped on light-sheet microscopy and provided advice. M.G. provided advice on CRISPR–Cas9 engineering. A.-M.G. and J.S. provided GTA002 cells. L.T.-R. and K.-J.M. performed experiments in ADAPT-NK. A. Rea and A.M. wrote the original draft. All authors discussed the results and commented on the paper.

Competing interests

A. Rea, M.S.-G. and A.M. are inventors of a filed patent (EP23383142, submitted 8 November 2023) pertaining to the results presented in the paper. The other authors declare no competing interests.

Additional information

Extended data is available for this paper at https://doi.org/10.1038/s41590-025-02103-z.

Supplementary information The online version contains supplementary material available at https://doi.org/10.1038/s41590-025-02103-z.

Correspondence and requests for materials should be addressed to Aura Muntasell.

Peer review information *Nature Immunology* thanks Enrico Maggi and the other, anonymous, reviewer(s) for their contribution to the peer review of this work. Peer reviewer reports are available. Primary Handling Editor: P. Jauregui, in collaboration with the *Nature Immunology* team.

https://doi.org/10.1038/s41590-025-02103-z

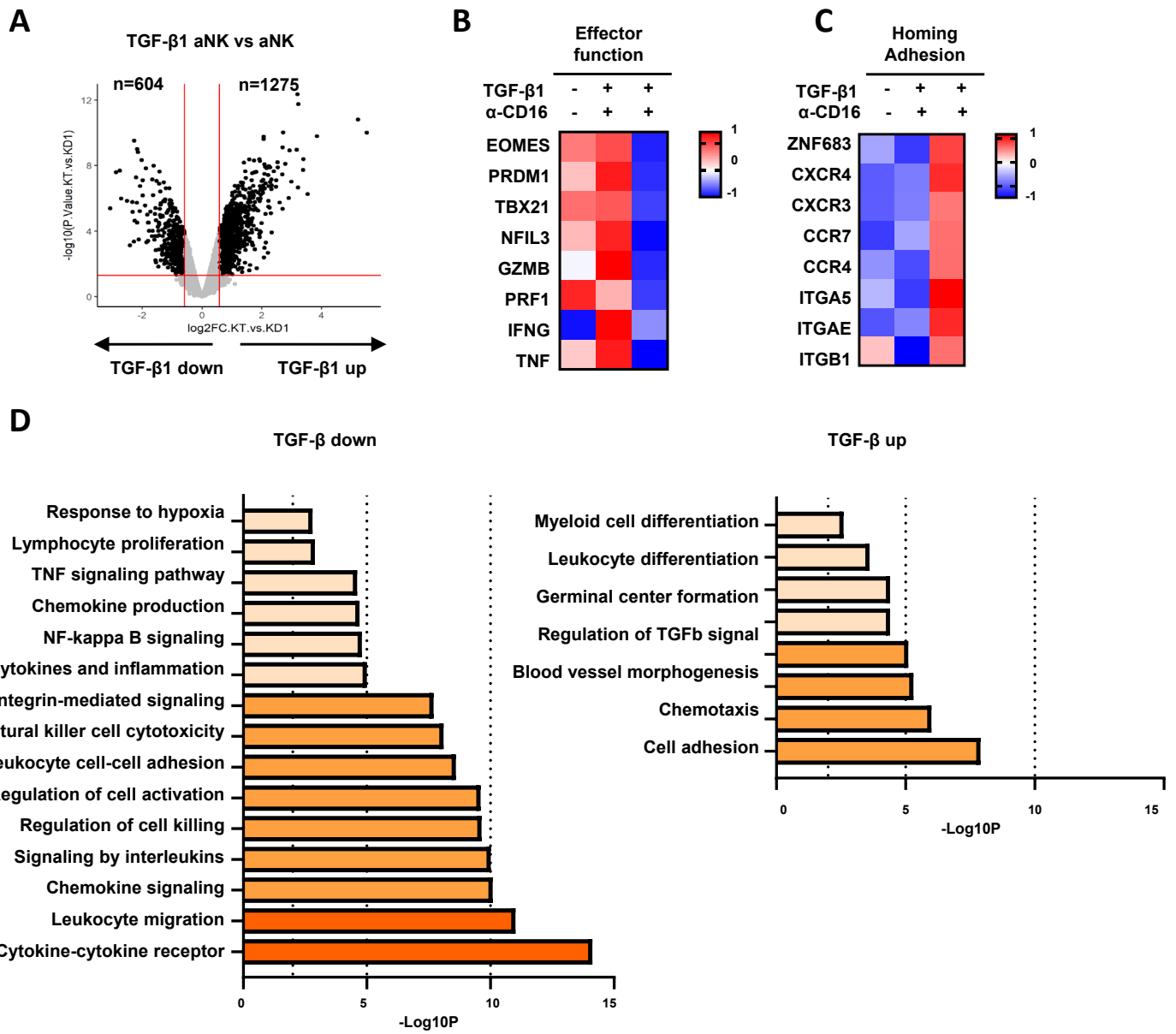

Extended Data Fig. 1 | Biological pathways modulated in TGF-β-treated NK cells. Reanalysis of publicly available microarray data of CD16-activated human NK cells in the presence or absence of TGF-β1 (GSE156200). **a, b, c**) Volcano plot and Heat Maps showing global and selected differential expressed genes (DEG) (|log fold-change|> or <0.5; pval <0.05). **d**) DEG in TGF-β1-treated versus non-treated activated NK cells were separately introduced in metascape software. Bar graph showing biological pathways down- or up-regulated in TGF-β1-treated NK cells.

https://doi.org/10.1038/s41590-025-02103-z

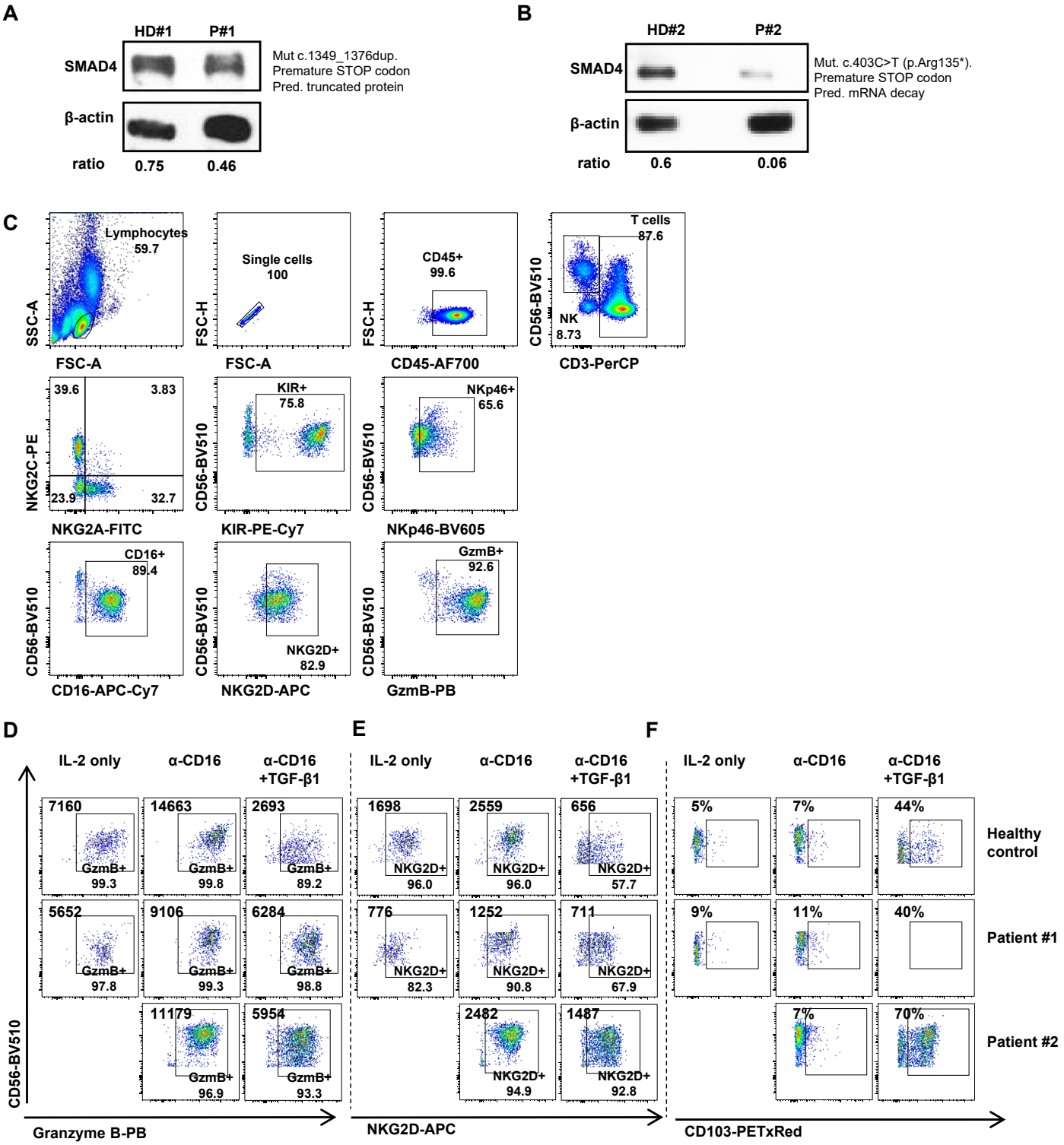

Extended Data Fig. 2 | SMAD4 expression and NK cell phenotype in PBMC from *SMAD4* haploinsufficient patients. a, b) SMAD4 and β-actin expression in fresh PBMC from two patients with juvenile polyposis syndrome (P#1, P#2) and two healthy donors (HD#1 and HD#2) by western blot. Mutations for each JPS patient are indicated. **c-f**) PBMC from a healthy donor and the two JPS patients were cultured on anti-CD16-coated plates with of IL-2 ± TGF-β1 for 6 days. **c**) Gating strategy and dot plots fo Granzyme B (**d**), NKG2D (**e**) and CD103 (**f**) expression as analysed by flow cytometry. Inset numbers indicate MFI for Granzyme B and NKG2D and percentages of CD103 + NK cells.

https://doi.org/10.1038/s41590-025-02103-z

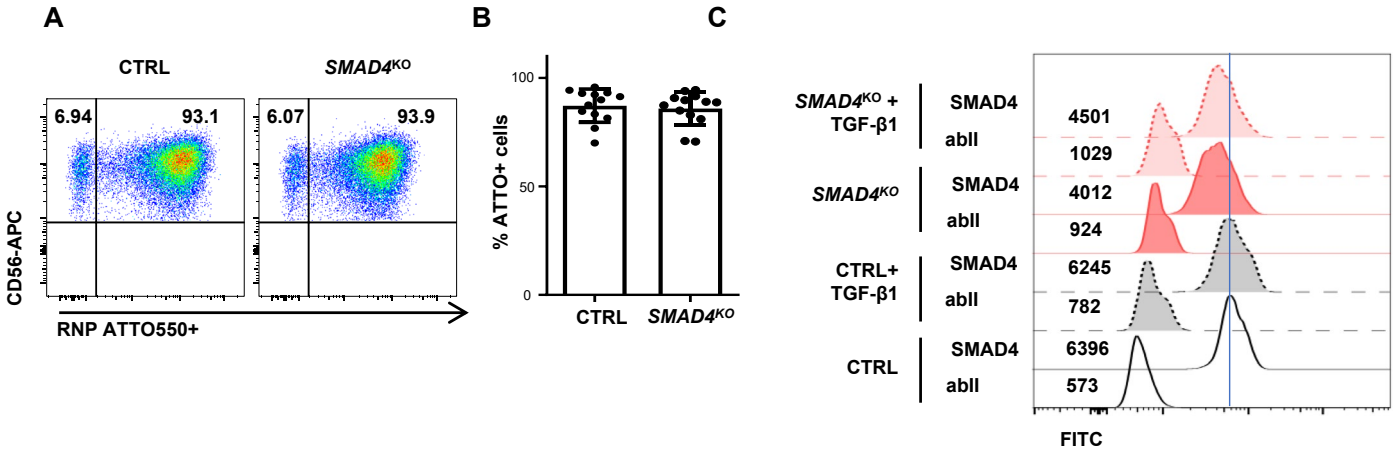

Extended Data Fig. 3 | Cas9 RNP nucleofection efficiency and SMAD4 reduction on primary human expanded NK cells. a-b) NK cells isolated at at day 7 post expansion were nucleofected with ATTO550-labeled sgRNA control or *SMAD4* gRNA complexed to Cas9. Monitorization of nucleofection efficiency after overnight culture by flow cytometry. **a**) Dot plot showing the percentage of nucleofected cells (ATTO550 +) in one representative nucleofection. **b**) Mean ± SEM nucleofection efficiency in 13 independent experiments. **c**) SMAD4 expression in NK cells after 7 days culture with IL-2 ± TGF-β as analysed by flow cytometry. Inset numbers indicate Mean fluorescence intensity. Histograms corresponding to the control staining with the secondary antibody (abII) for every condition are shown. Data from one representative experiment.

https://doi.org/10.1038/s41590-025-02103-z

A

```
DCTN5:                      CREBBP:                     NUFIP2:

AAGGCGGGCGGATCACTTGAggg     CAAAGTATGTGATTACCTGGggg     GAAGCAGAAGGATCACTTGAggg
..........|||.|||||.        ...|.|....||||||||||       |..|..|.|.|||.|||||.
GTCGATGCACGATTACTTGGtgg      GTCGATGCACGATTACTTGGtgg      GTCGATGCACGATTACTTGGtgg
```

B

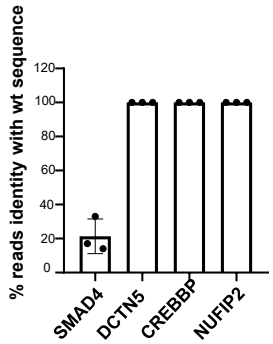

Extended Data Fig. 4 | Analysis of off-target gene editing. a) Alignment of *SMAD4* crRNA with putative off-target events. PAM is indicated in lower case. **b)** Bar graphs showing the percentage of sequenced reads with identical alignment to SMAD4 or to the potential off-target genes DCTN5, CREBBP and NUFIP2 as analysed in *SMAD4*^{KO} NK cells. Each dot represents data from SMAD4^{KO} NK cells from different individuals (n = 3).

https://doi.org/10.1038/s41590-025-02103-z

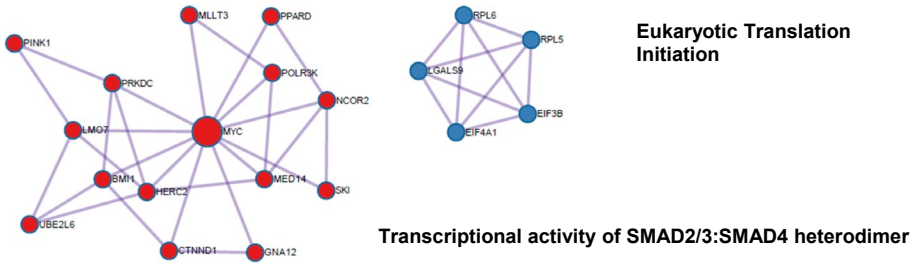

Extended Data Fig. 5 | Biological pathways down-regulated in *SMAD4*^{KO} NK cells. Biological pathways down-regulated in *SMAD4*^{KO} as compared to control-engineered expanded NK cells according to Metascape unsupervised analysis.

https://doi.org/10.1038/s41590-025-02103-z

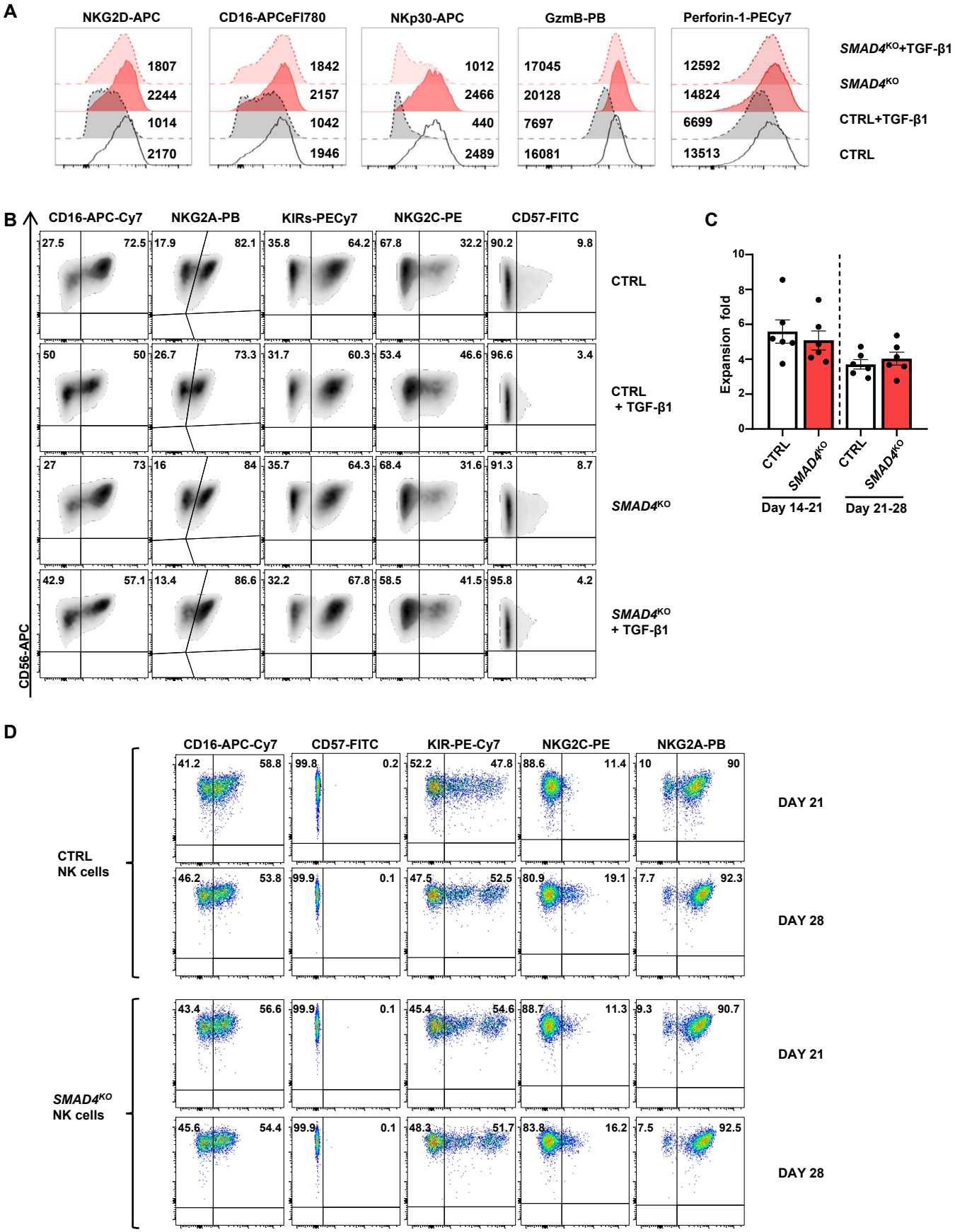

Extended Data Fig. 6 | See next page for caption.

https://doi.org/10.1038/s41590-025-02103-z

Extended Data Fig. 6 | Extended phenotype of control and SMAD4^{KO} NK cells treated or ot with TGF-β. Expression of NK cell receptors and effector molecules in control and SMAD4^{KO} NK treated with Il-2 ± TGF-β1 were analyzed by flow cytometry. **a**) Histograms showing the expression of surface NKG2D, CD16, NKp30 and intracellular granzyme B (GzmB) and perforin-1 in NK cells from a representative donor. **b**) Density plots showing the surface expression of CD16, NKG2A, KIR, NKG2C and CD57 in control- and SMAD4^{KO} NK cells of a representative donor. Expansion fold (**c**) and phenotype (**d**) of control and *SMAD4*^{KO} NK cells in two consecutive restimulations with K562-CD137L-IL15tmb-IL21tmb feeder cells.

https://doi.org/10.1038/s41590-025-02103-z

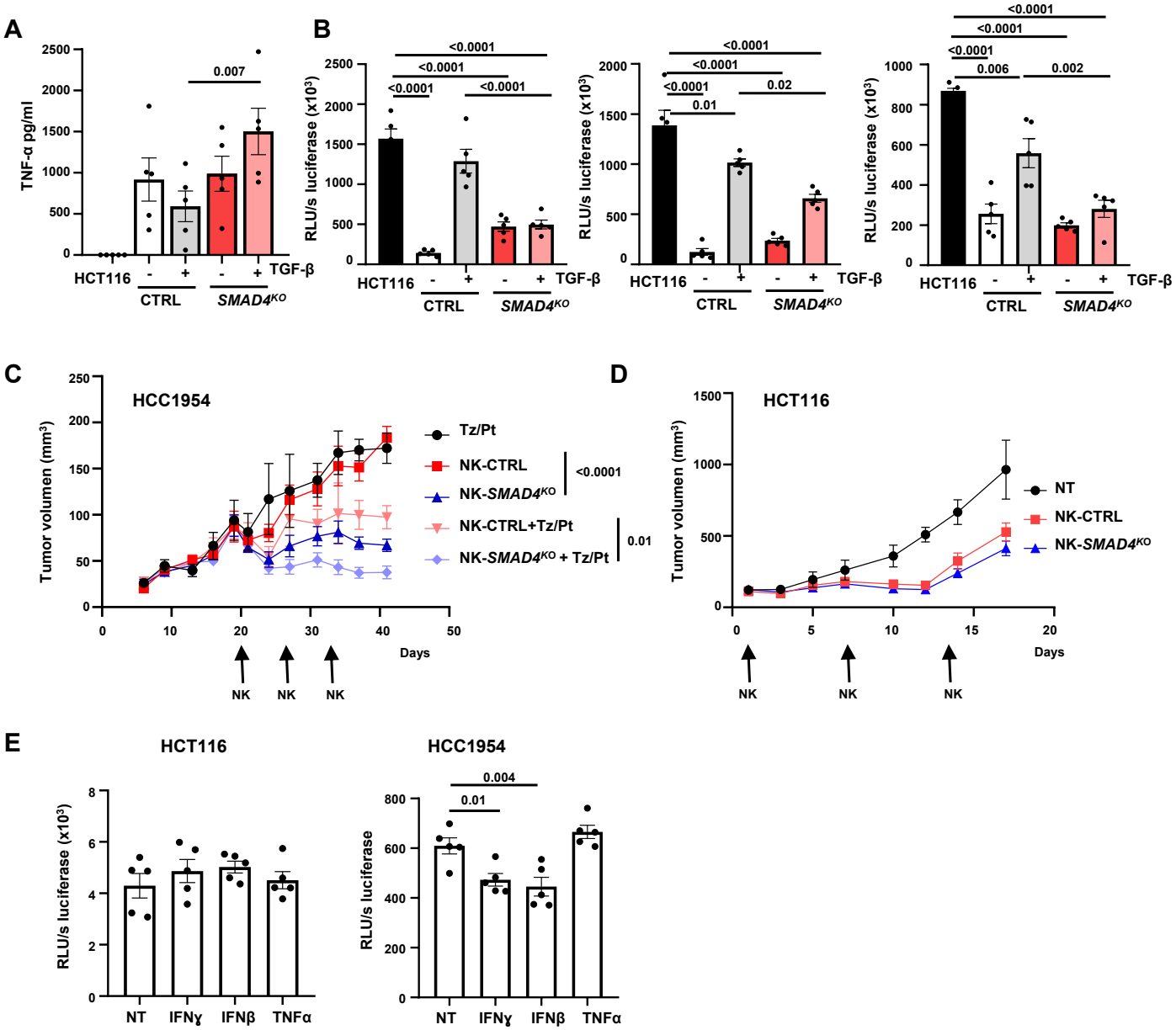

Extended Data Fig. 7 | Function of control and *SMAD4*^{KO} NK cells treated or not with TGF-β. a) Mean ± SEM TNF in culture supernatants of control- and *SMAD4*^{KO} NK cells after 2 h coculture with HCT116 cells as analysed by ELISA. Statistical significance calculated by one-way ANOVA followed by Fisher's test. **b**) HCT116-Luc + -GFP+ spheroids were cocultured with control- or *SMAD4*^{KO} NK cells previously treated with IL-2 ± TGF-β. Mean ± SEM Luciferase activity of remaining HCT116 cells after 24 h coculture. Data from 3 independent experiments using NK cells from different donors. Each dot represents data from the 5 technical replicates included in each condition. Statistical significance calculated by one-way ANOVA followed by Turkey's multiple comparisons test. **c**) HCC1954 xenografts in NSG mice were treated with either: i) trastuzumab (Tz)/pertuzumab (Pt)(n = 4); ii) control NK cells (2×10^5,n = 5); iii) SMAD4^{KO} NK cells (2×10^5,n = 5); iv) control NK cells (1×10^5) and trastuzumab/pertuzumab (n = 5) or v) SMAD4^{KO} NK cells (1×10^5) and trastuzumab/pertuzumab (n = 5). Tumor volume in each treatment group. Statistical significance between control and SMAD4^{KO} NK cells treatments at the last measurment by two-way ANOVA followed by Turkey's multiple comparisons test are indicated. **d**) HCT116 xenografts in NSG mice were treated with either control or SMAD4^{KO} NK cells (2×10^5). Tumor volume in each treatment group (n = 5 in NT and n = 6 in NK cell treated groups). **e**) HCT116-GFP + -Luc+ and HCC1954 GFP + -Luc+ spheroids were cultured with rIFNγ, rIFN-β or rTNF. Mean ± SEM Luciferase activity of HCT116 nd HCC1954 spheroids after 24 h coculture. Statistical significance by one-way ANOVA followed by Turkey's multiple comparisons test.

https://doi.org/10.1038/s41590-025-02103-z

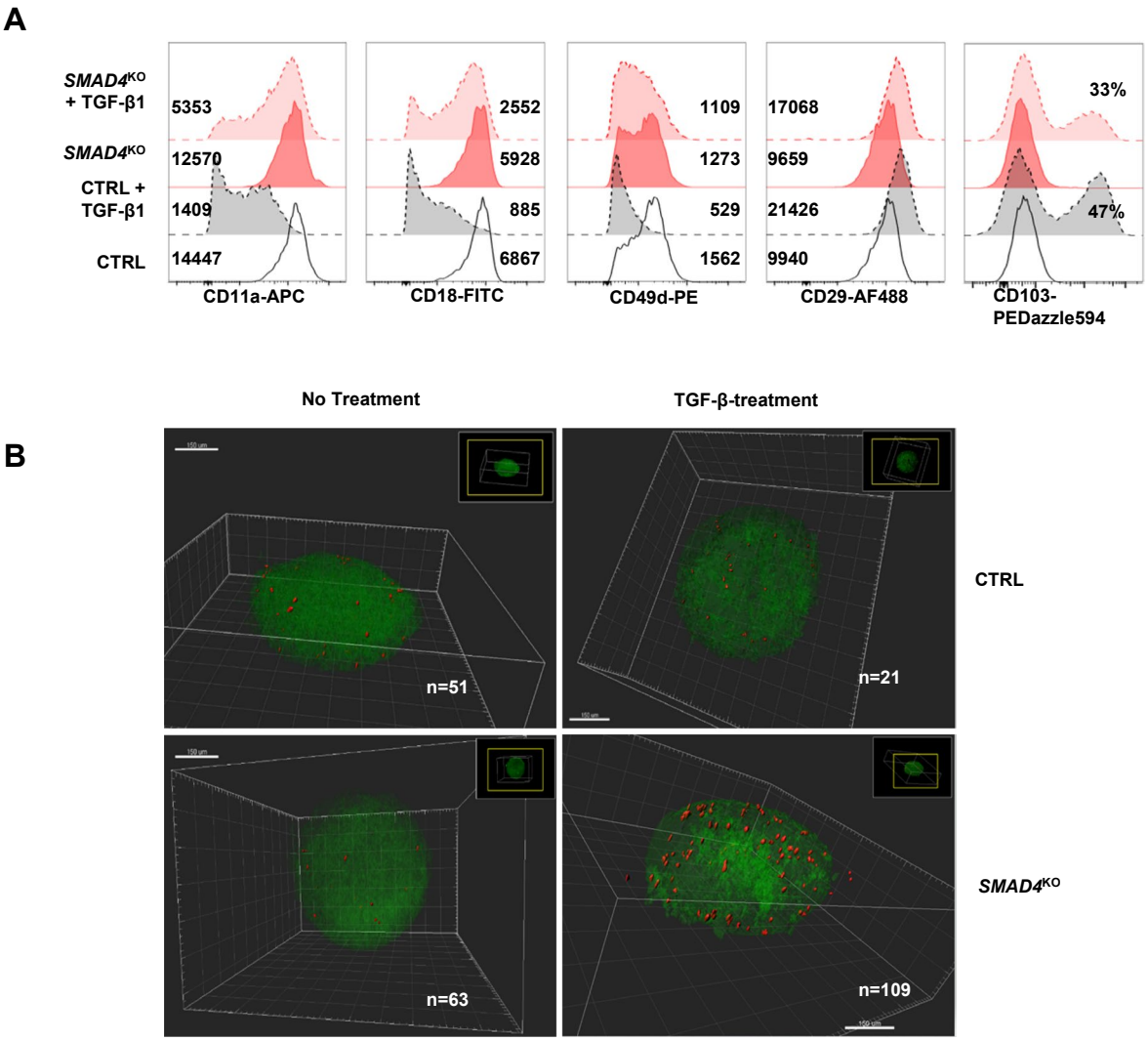

Extended Data Fig. 8 | Impact of SMAD4 and TGF-β in the integrin profile of expanded NK cells. a) Surface expression of LFA-1 (CD11a and CD18), VLA-4 (CD49d and CD29) and CD103 in control and *SMAD4*^{KO} NK cells treated with IL-2 ± TGF-β as analysed by flow cytometry. Representative histograms of each marker staining in NK cells from a representative individual. **b**) HCT116 spheroids were cocultured with control- or *SMAD4*^{KO} NK cells previously treated with IL2 ± TGF-β. After 1 h coculture, spheroids and attached NK cells were fixed and processed for lightsheet imaging. HCT116 cells were labeled with an anti-Epcam-FITC antibody and NK cells with an anti-CD45-VioR667 antibody. Image of a representative HCT116 spheroid for the indicated conditions. Inset numbers correspond to the number of NK cells counted in each spheroid.

https://doi.org/10.1038/s41590-025-02103-z

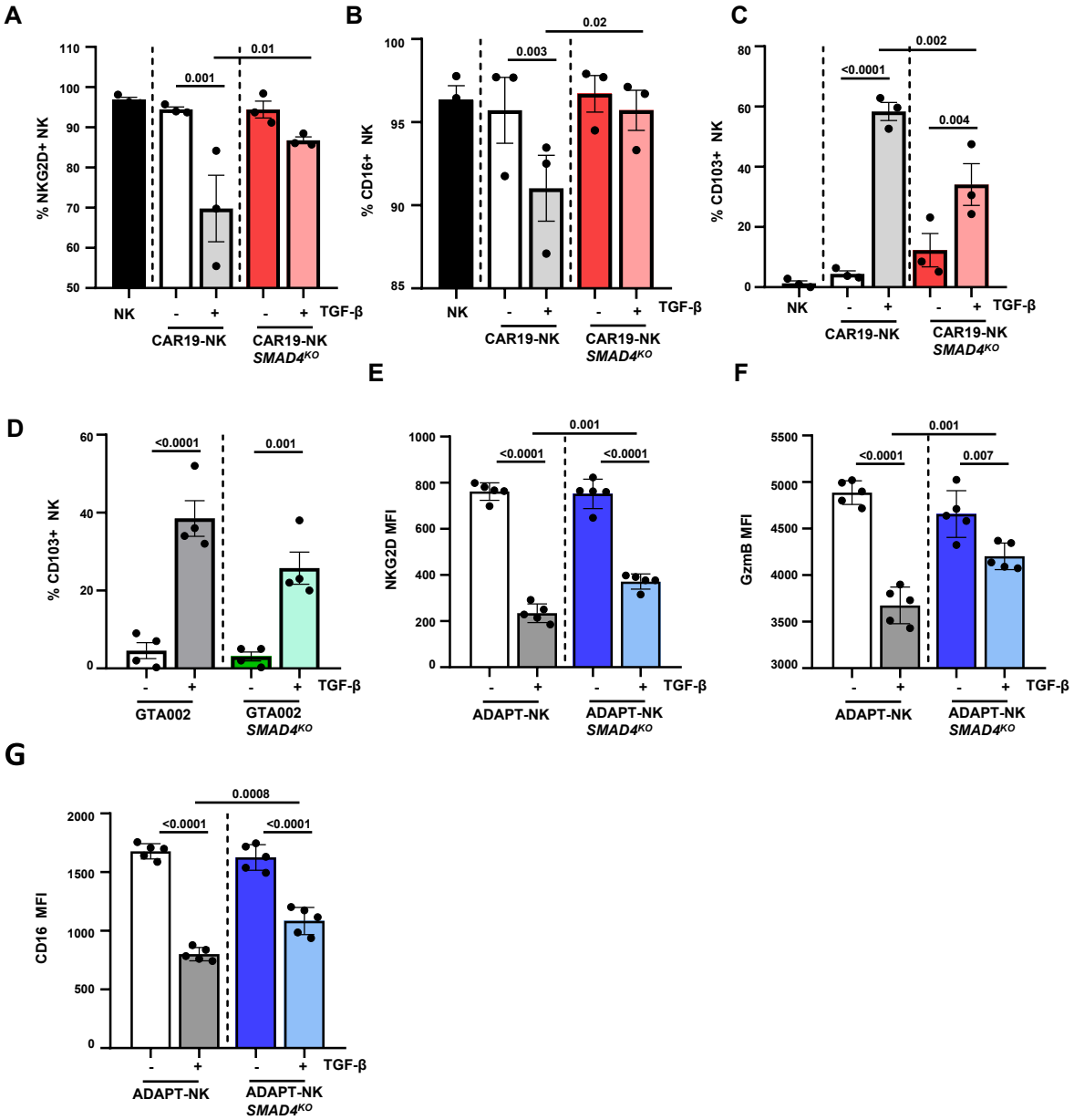

Extended Data Fig. 9 | Influence of *SMAD4* knock out on CAR19-NK, GTA002 and ADAPT-NK cell products exposed or not to TGF-β. a-c) Mean ± SEM percentatge of NKG2D+, CD16+ and CD103+ control and SMAD4^{KO} CAR19 NK cells in the indicated conditions **d**) Mean ± SEM percentatge of CD103+ control and SMAD4^{KO} GTA002 cells in the indicated conditions. **e-f**) Mean ± SEM percentatge of NKG2D+, CD16+ and CD103+ control and SMAD4^{KO} ADAPT-NK cells in the indicated conditions. Dots show data of independent experiments performed with NK cells from diferent donors. Statistical significance one-way ANOVA followed by Fisher'stest in A, B and C; and one-way ANOVA followed by Turkey's multipe comparisons test in **d-g**.

nature portfolio

Corresponding author(s): Aura Muntasell

Last updated by author(s): 20/01/2025

Reporting Summary

Nature Portfolio wishes to improve the reproducibility of the work that we publish. This form provides structure for consistency and transparency in reporting. For further information on Nature Portfolio policies, see our Editorial Policies and the Editorial Policy Checklist.

Statistics

For all statistical analyses, confirm that the following items are present in the figure legend, table legend, main text, or Methods section.

n/a	Confirmed
☐	☒ The exact sample size (*n*) for each experimental group/condition, given as a discrete number and unit of measurement
☐	☒ A statement on whether measurements were taken from distinct samples or whether the same sample was measured repeatedly
☐	☒ The statistical test(s) used AND whether they are one- or two-sided *Only common tests should be described solely by name; describe more complex techniques in the Methods section.*
☒	☐ A description of all covariates tested
☐	☒ A description of any assumptions or corrections, such as tests of normality and adjustment for multiple comparisons
☐	☒ A full description of the statistical parameters including central tendency (e.g. means) or other basic estimates (e.g. regression coefficient) AND variation (e.g. standard deviation) or associated estimates of uncertainty (e.g. confidence intervals)
☒	☐ For null hypothesis testing, the test statistic (e.g. *F*, *t*, *r*) with confidence intervals, effect sizes, degrees of freedom and *P* value noted *Give P values as exact values whenever suitable.*
☒	☐ For Bayesian analysis, information on the choice of priors and Markov chain Monte Carlo settings
☒	☐ For hierarchical and complex designs, identification of the appropriate level for tests and full reporting of outcomes
☒	☐ Estimates of effect sizes (e.g. Cohen's *d*, Pearson's *r*), indicating how they were calculated

Our web collection on statistics for biologists contains articles on many of the points above.

Software and code

Policy information about availability of computer code

Data collection	Fortessa or LSRII flow cytometers were used for flow cytometry data collecion. Luminescence was measured at FB12 Tube Luminometer (Berthold Technologies) or at Orion II Microplate Luminometer (Berthold Technologies).Fluorescence images were acquired using Zeiss Cell Observer HS microscope. UltraMicroscope Blaze (Miltenyi Biotec) was used for light sheet imaging. RNA sequencing was performed with NextSeq High output, Illumina. On target and off target gene editing was analysed in by miSeq Illumina.
Data analysis	Protospacer sequences targeting SMAD4 gene were identified using the CRISPRscan algorithm. FlowJo X software (FlowJo v10.8.1, LLC) was used for flow cytometry data analyis. Images were quantified by signal quantified by ImageJ software (v54a) or Imaris® software (10.0). Metascape software (3.1.3) was used for gene annotation and analysis.Reads were mapped with STAR (version 2.5.9a) against the human reference from Ensembl (version GRCh38), and counts were obtained with HTSeq (version 0.9.1). MultiQC (version 1.9) was used for Quality Control assessment. DESeq2 and limma R packages (version 4.0.0) were used for the analysis of differentially expressed genes (DEG). Gene set enrichment analysis (GSEA) was performed by R package ¨clusterProfiler¨ package version 4.0.0 .CRISPRroots tool (v1.2) was used for off-target assessment in CRISPR–Cas9 edited cells. CRISPR-Analytics platform (https://synbio.upf.edu/crispr-a/ which runs nextflow pipeline https://bitbucket.org/synbiolab/crispr-a_nextflow/. Commit: a297a2d) was used for the nalysis of on target and off-target edditing. Statistics were calculated using GraphPad Prism (v8.0) or in R base and R package edgeR (v 3.22.3).

For manuscripts utilizing custom algorithms or software that are central to the research but not yet described in published literature, software must be made available to editors and reviewers. We strongly encourage code deposition in a community repository (e.g. GitHub). See the Nature Portfolio guidelines for submitting code & software for further information.

Data

Policy information about availability of data

All manuscripts must include a data availability statement. This statement should provide the following information, where applicable:

- Accession codes, unique identifiers, or web links for publicly available datasets
- A description of any restrictions on data availability
- For clinical datasets or third party data, please ensure that the statement adheres to our policy

Processed bulk RNA-seq data are available through the Gene Expression Omnibus (GEO) under accession number GSE248292. Raw data on SMAD4 exon 5 amplimers and putative off-target gene sequences are available at ENA under accession number PRJEB70283.
The K562-CD137L-IL15tm-IL21tm was provided under material transfer agreement between Georg-Speyer-Haus and St. Jude Children's Research Hospital with IMIM- Hospital del Mar Medical Research Institute. GTA002 cells were provided under material transfer agreement between Glycostem and IMIM- Hospital del Mar Medical Research Institute. All other data needed to evaluate the conclusions in the paper are present in the paper, source data or the Supplementary Information Data involving human research participants are subject to the data protection constraints in the written informed consent signed by the student participants.

Research involving human participants, their data, or biological material

Policy information about studies with human participants or human data. See also policy information about sex, gender (identity/presentation), and sexual orientation and race, ethnicity and racism.

Reporting on sex and gender	Research findings do not apply to one sex or gender
Reporting on race, ethnicity, or other socially relevant groupings	Research findings do not apply to any race, ethnicity or socially relevant group
Population characteristics	Research findings do not apply to any popultion characteristics.
Recruitment	Blood samples were obtained from healthy volunteer donors and two Juvenile Polyposis syndrome patients upon written informed consent. Volunteers did not received any compensation for participating in the study.
Ethics oversight	Experiments involving expansion of adaptive NK cells from healthy donors were approved by the regional ethics committee in Norway (Regional etisk komité (REK): 2018/2482) and the Clinical Research Ethics Committee, Parc de Salut Mar (nº 2018/787/I). Studies on JPS patients were approved by the Clinical Research Ethics Committee at Hospital Clínic de Barcelona (nº HCB/2020/0290). Written informed consent was obtained from all participants and the study adhered to the Declaration of Helsinki.

Note that full information on the approval of the study protocol must also be provided in the manuscript.

Field-specific reporting

Please select the one below that is the best fit for your research. If you are not sure, read the appropriate sections before making your selection.

☒ Life sciences ☐ Behavioural & social sciences ☐ Ecological, evolutionary & environmental sciences

For a reference copy of the document with all sections, see nature.com/documents/nr-reporting-summary-flat.pdf

Life sciences study design

All studies must disclose on these points even when the disclosure is negative.

Sample size	Sample sizes are noted for each experiment in the relevant figure legends. Samples sizes were estimated based on prior experience (PMID38167224, PMID34580116). For JPS patient's studies samles size was limited by number of patients available.
Data exclusions	No data were excluded from any analyses.
Replication	Biological replicates (i.e. samples from different research participants or animals) were included for all ex vivo culture experiments. Technical replicates (i.e. repeated measurements of the same sample) have been indicated. For all ELISA-samples were tested in triplicate and no data was excluded.
Randomization	For in vitro experiments, cells were randomized allocated to groups. For in vivo experiments, mice were randomized allocated to groups based on tumor burden at the time of treatment.
Blinding	In RNAseq and illumina sequencing analysis investigators were blinded to the treatment conditions, In in vitro and NSG mice experiments Investigators were not blinded to the treatment.Mice were randomly tag in the ear at experiment was set up. we recognized each mouse by

the ear tag when acquiring data. Blinding was not necessary as no data was excluded and only objective measurable criteria were used for this study

Reporting for specific materials, systems and methods

We require information from authors about some types of materials, experimental systems and methods used in many studies. Here, indicate whether each material, system or method listed is relevant to your study. If you are not sure if a list item applies to your research, read the appropriate section before selecting a response.

Materials & experimental systems

n/a	Involved in the study
☐	☒ Antibodies
☐	☒ Eukaryotic cell lines
☒	☐ Palaeontology and archaeology
☐	☒ Animals and other organisms
☒	☐ Clinical data
☒	☐ Dual use research of concern
☒	☐ Plants

Methods

n/a	Involved in the study
☒	☐ ChIP-seq
☐	☒ Flow cytometry
☒	☐ MRI-based neuroimaging

Antibodies

Antibodies used

Anti-human Active caspase 3-FITC C92-605 BD Bioscience, 559341, 1:12
Anti-human CCR5-APC J418F1 Biolegend, 359122, 1:25
Anti-human CD3-PerCP SK7 BD Bioscience, 345766, 1:12
Anti-human CD3-PerCP SPV.T3b, Dr. J. de Vries, labeled at Immunostep, 1:100
Anti-human CD11a-APC HI111 Biolegend, 301212, 1:12
Anti-human CD16-APC-eFluor 780 CB16 eBioscience, 47-0168-42, 1:50
Anti-human CD29-Alexa Fluor 488 TS2/16 Biolegend, 303016, 1:25
Anti-human CD45-Alexa Fluor 700 2D1 eBioscience, 56-9459-42, 1:50
Anti-human CD45- Vio® R667, REA747, Miltenyi, 130-128-742, 10ug/mL
Anti-human Epcam-Alexa Fluor 488, policlonal, abcam, ab237395, 5ug/ml
Anti-human CD49d-PE 9F10 Biolegend, 304304, 1:25
Anti-human CD56-APC CMSSB eBioscience, 17-0567-42, 1:25
Anti-human CD56-BV10 NCAM16.2 BD Bioscience, 563041, 1:12
Anti-human CD57-APC HCD57 Biolegend, 359610 , 1:50
Anti-human CD103-PE/Dazzle 594 Ber-ACT8 Biolegend, 350224, 1:25
Anti-human CD107a-FITC H4A3 BD Bioscience, 555800, 1:12
Anti-human CXCR3-eFluor 660 CEW33D eBioscience, 50-1839-42, 1:12
Anti-human CXCR3-PE G025H7 Biolegend, 353706, 1:12
Anti-human CXCR4-PE 1D9 BD Bioscience, 551510, 1:12
Anti-human Granzyme B-Pacific Blue GB11 Biolegend, 515408, 1:12
Anti-human KLRG1-BV605 2F1 Biolegend, 138419, 1:12
Anti-human NKG2A-FITC, Z199 Dr. A Moretta, labeled in the lab 1:200
Anti-human NKG2A-CF-Blue Z199 Dr. A Moretta, labeled at Immunostep, 1:100
Anti-human NKG2C-PE FAB138P R&D systems, 134591, 1:25
Anti-human NKG2D-APC BAT221 Miltenyi Biotec, 130-092-673, 1:40
Anti-human NKp30-APC REA823 Miltenyi Biotec, 130-121-995, 1:25
Anti-human NKp46-BV605 9E2 Biolegend, 331926, 1:25
Anti-human Perforin dG9 Biolegend, 308126, 1:12
Anti-human SMAD4 D3R4N Cell signaling, 46535S, 1:100 FACS, 1:1000 WB
CD19 CAR detection reagent, rhumanIgG1 Miltenyi, 130-129-550, 1:50
Anti-human CD14-APC M5E2 BD Bioscience 561383 1:25
Anti-human CD19-PE SJ25C1 BD Bioscience 340364 1:25
Anti-human IFNɣ-APC B27 BD Bioscience 554702 1:50
Anti-human TNF-α-CF Blue Infliximab Jannsen, labeled at Immunostep, 1:100
anti-mouse IgG-PE-Cy7 Poly4053 Biolegend 405315 1:50
anti-mouse IgG-FITC Polyclonal Agilent Technologies F0261 1:100
anti-rabbit IgG Alexa Fluor® 488 Polyclonal Jackson Immunoresearch 111-545-003 1:500
Anti-human -Phospho-Smad2 (Ser465/467) 138D4 Cell Signaling 3108S 1:1000
Anti-human -Smad7 293039 R&D System MAB2029 1:1000
Anti-human -TGFβ-RII C4 Santa Cruz Biotechnology sc-17791 1:100
Anti-human -TIF1gamma Polyclonal Bethyl Laboratories, Inc A301-060A 1:1000
Anti-human -β-actin AC-15 Sigma-Aldrich A5441 1:20000

Hybridoma supernatants:
Anti-human CD18 TS1/18 Dr. F. Sánchez-Madrid 1:2
Anti-human KIR2DL1, -2DS1/S3/S5 HPMA-4 Dr. M. López-Botet 1:5
Anti-human KIR2DL2/L3, -2DS2 CHL Dr. S Ferrini 1:5
Anti-human KIR2DL5 UP-R1 Dr. M. López-Botet 1:5

Anti-human KIR2DL1/L2, -2DS2/S4/S5, -3DS1 5.133 Dr. M. Colonna 1:5
Anti-human KIR3DL1 DX9 Dr. L Lanier 1:5

Validation

All antibodies were purchased from commercial suppliers (BD Biosciences, BioLegend, ThermoFisher). Validation statement were confirmed from the manufacturers' website for their relevant used in the study:
Anti-human Active caspase 3-FITC https://www.bdbiosciences.com/en-ie/products/reagents/flow-cytometry-reagents/research-reagents/single-color-antibodies-ruo/fitc-rabbit-anti-active-caspase-3.559341?tab=product_details
Anti-human CCR5-APC https://www.biolegend.com/nl-be/products/apc-anti-human-cd195-ccr5-antibody-10241
Anti-human CD3-PerCP SK7 BD Bioscience, 345766, 1:12
https://www.bdbiosciences.com/en-eu/products/reagents/flow-cytometry-reagents/clinical-diagnostics/single-color-antibodies-asr-ivd-ce-ivd/cd3-percp.345766?tab=product_details
Anti-human CD11a-APC HI111 Biolegend, 301212, 1:12
https://www.biolegend.com/en-gb/products/apc-anti-human-cd11a-antibody-693?GroupID=BLG11947
Anti-human CD16-APC-eFluor 780 CB16 eBioscience, 47-0168-42, 1:50
https://www.thermofisher.com/antibody/product/CD16-Antibody-clone-eBioCB16-CB16-Monoclonal/47-0168-42
Anti-human CD29-Alexa Fluor 488 TS2/16 Biolegend, 303016, 1:25
https://www.biolegend.com/nl-be/products/alexa-fluor-488-anti-human-cd29-antibody-3257?GroupID=BLG10310
Anti-human CD45-Alexa Fluor 700 2D1 eBioscience, 56-9459-42, 1:50
https://www.thermofisher.com/antibody/product/CD45-Antibody-clone-2D1-Monoclonal/56-9459-42
Anti-human CD45- Vio® R667, REA747, Miltenyi, 130-128-742, 10ug/mL
https://www.miltenyibiotec.com/ES-en/products/cd45-antibody-anti-human-reafinity-rea747.html#conjugate=vio-r667:size=600-ul
Anti-human Epcam-Alexa Fluor 488, policlonal, abcam, ab237395, 5ug/ml
https://www.abcam.com/en-us/products/primary-antibodies/alexa-fluor-488-epcam-antibody-epr20532-225-ab237395
Anti-human CD49d-PE 9F10 Biolegend, 304304, 1:25
https://www.biolegend.com/ja-jp/products/pe-anti-human-cd49d-antibody-584
Anti-human CD56-APC CMSSB eBioscience, 17-0567-42, 1:25
https://www.thermofisher.com/antibody/product/CD56-NCAM-Antibody-clone-CMSSB-Monoclonal/17-0567-42
Anti-human CD56-BV10 NCAM16.2 BD Bioscience, 563041, 1:12
https://www.bdbiosciences.com/en-es/products/reagents/flow-cytometry-reagents/research-reagents/single-color-antibodies-ruo/bv510-mouse-anti-human-cd56.563041?tab=product_details
Anti-human CD57-APC HCD57 Biolegend, 359610, 1:50
https://www.biolegend.com/nl-be/products/apc-anti-human-cd57-antibody-9023
Anti-human CD103-PE/Dazzle 594 Ber-ACT8 Biolegend, 350224, 1:25
https://www.biolegend.com/nl-be/products/pedazzle-594-anti-human-cd103-integrin-alphae-antibody-14940?GroupID=BLG15664
Anti-human CD107a-FITC H4A3 BD Bioscience, 555800, 1:12
https://www.bdbiosciences.com/en-lu/products/reagents/flow-cytometry-reagents/research-reagents/single-color-antibodies-ruo/fitc-mouse-anti-human-cd107a.555800?tab=product_details
Anti-human CXCR3-eFluor 660 CEW33D eBioscience, 50-1839-42, 1:12
https://www.thermofisher.com/antibody/product/CD183-CXCR3-Antibody-clone-CEW33D-Monoclonal/50-1839-42
Anti-human CXCR3-PE G025H7 Biolegend, 353706, 1:12
https://www.biolegend.com/nl-be/products/pe-anti-human-cd183-cxcr3-antibody-7579
Anti-human CXCR4-PE 1D9 BD Bioscience, 551510, 1:12
https://www.bdbiosciences.com/en-us/products/reagents/flow-cytometry-reagents/research-reagents/single-color-antibodies-ruo/pe-rat-anti-human-cd184.551510?tab=product_details
Anti-human Granzyme B-Pacific Blue GB11 Biolegend, 515408, 1:12
https://www.biolegend.com/ja-jp/products/pacific-blue-anti-human-mouse-granzyme-b-antibody-8612
Anti-human KLRG1-BV605 2F1 Biolegend, 138419, 1:12
https://www.biolegend.com/en-gb/products/brilliant-violet-605-anti-mouse-human-klrg1-mafa-antibody-9644?GroupID=BLG8908
Anti-human NKG2C-PE 134591 R&D systems, FAB138P, 1:25
https://www.rndsystems.com/products/human-nkg2c-cd159c-pe-conjugated-antibody-134591_fab138p
Anti-human NKG2D-APC BAT221 Miltenyi Biotec, 130-092-673, 1:40
https://www.miltenyibiotec.com/ES-en/products/cd314-nkg2d-antibody-anti-human-bat221.html#conjugate=apc:size=100-tests-in-200-ul (Ha cambiado y ahora es ref 130-117-718)
Anti-human NKp30-APC REA823 Miltenyi Biotec, 130-121-995, 1:25
https://www.miltenyibiotec.com/ES-en/products/cd337-nkp30-antibody-anti-human-af29-4d12.html#conjugate=apc:size=100-tests-in-200-ul
Anti-human NKp46-BV605 9E2 Biolegend, 331926, 1:25
https://www.biolegend.com/en-gb/sean-tuckers-tests/brilliant-violet-605-anti-human-cd335-nkp46-antibody-8706?GroupID=BLG8494
Anti-human Perforin dG9 Biolegend, 308126, 1:12
https://www.biolegend.com/de-at/products/pe-cyanine7-anti-human-perforin-antibody-13094
Anti-human SMAD4 D3R4N Cell signaling, 46535S, 1:100 FACS, 1:1000 WB
https://www.cellsignal.com/products/primary-antibodies/smad4-d3r4n-xp-rabbit-mab/46535?srsltid=AfmBOoq9NGNL75H4wrtKSqTkrX9oUjfZ1c7G0pAoFumtO9ZAkl6GWuaI
CD19 CAR detection reagent, rhumanIgG1 Miltenyi, 130-129-550, 1:50
https://www.miltenyibiotec.com/ES-en/products/cd19-car-detection-reagent-human.html
Anti-human CD14-APC M5E2 BD Bioscience 561383 1:25
https://www.bdbiosciences.com/en-us/products/reagents/flow-cytometry-reagents/research-reagents/single-color-antibodies-ruo/apc-mouse-anti-human-cd14.561383?tab=product_details
Anti-human CD19-PE SJ25C1 BD Bioscience 340364 1:25
https://www.bdbiosciences.com/en-us/products/reagents/flow-cytometry-reagents/clinical-discovery-research/single-color-antibodies-ruo-gmp/pe-mouse-anti-human-cd19.340364?tab=product_details
Anti-human IFNɣ-APC B27 BD Bioscience 554702 1:50
https://www.bdbiosciences.com/en-us/products/reagents/flow-cytometry-reagents/research-reagents/single-color-antibodies-ruo/

apc-mouse-anti-human-ifn.554702?tab=product_details
anti-mouse IgG-PE-Cy7 Poly4053 Biolegend 405315 1:50
https://www.biolegend.com/en-gb/search-results/pe-cyanine7-goat-anti-mouse-igg-minimal-x-reactivity-6952?GroupID=GROUP23
anti-mouse IgG-FITC Polyclonal Agilent Technologies F0261 1:100
https://www.agilent.com/en/product/immunohistochemistry/antibodies-controls/secondary-antibodies/rabbit-anti-mouse-immunoglobulins-fitc-(solid-phase-absorbed)-153254
anti-rabbit IgG Alexa Fluor® 488 Polyclonal Jackson Immunoresearch 111-545-003 1:500
https://www.jacksonimmuno.com/catalog/products/111-545-003
Anti-human -Phospho-Smad2 (Ser465/467) 138D4 Cell Signaling 3108S 1:1000
https://www.cellsignal.com/products/primary-antibodies/phospho-smad2-ser465-467-138d4-rabbit-mab/3108
Anti-human -Smad7 293039 R&D System MAB2029 1:1000
https://www.rndsystems.com/products/human-mouse-rat-smad7-antibody-293039_mab2029
Anti-human -TGFβ-RII C4 Santa Cruz Biotechnology sc-17791 1:100
https://www.scbt.com/es/p/tgfbeta-rii-antibody-c-4?srsltid=AfmBOor41p4zQZYnDVFV07O683AdzrrUP_AeiezprgzTgunpFaYcvmt9
Anti-human -TIF1gamma Polyclonal Bethyl Laboratories, Inc A301-060A 1:1000
https://www.fortislife.com/products/primary-antibodies/rabbit-anti-trim33-tif1gamma-antibody/BETHYL-A301-060
Anti-human -β-actin AC-15 Sigma-Aldrich A5441 1:20000
https://www.sigmaaldrich.com/ES/es/product/sigma/a5441
Anti-human CD18 clone TS1/18
https://www.miltenyibiotec.com/DE-en/products/cd18-antibody-anti-human-ts1-18.html#conjugate=fitc:size=100-tests-in-200-ul
Anti-human KIR2DL1, -2DS1/S3/S5 HPMA-4 and the Anti-human KIR2DL1/L2, -2DS2/S4/S5, -3DS1 clone 5.133 in PMID: 24173145, the Anti-human KIR2DL2/L3, -2DS2 clone CHL in PMID: 30381896, the Anti-human KIR2DL5 clone UP-R1 in https://doi.org/10.4049/jimmunol.178.7.4402, the Anti-hum an KIR3DL1 clone DX9 in PMID: 17301953 and the anti-human NKG2A clone z199 in https://doi.org/10.1002/eji.1830261032, the anti-human CD3 clone SPV.T3b in PMID: 6332061

Eukaryotic cell lines

Policy information about cell lines and Sex and Gender in Research

Cell line source(s)	The K562 (CRL-3344), HCT116 (CCL247EMT) and HCC1954 (CRL-2338) cell lines were purchased from American Type Culture Collection (ATCC), the 8866 B-LCL and Nalm-6-GFP+-Luc+ cells were kindly provided by Dr. Miguel López-Botet (Universitat Pompeu Fabra) and Dr. Manel Juan (Hospital Clínic de Barcelona), respectively. HCT116-GFP+-Luc+ cells were kindly provided by Dr. Julian Pardo (Universidad de Zaragoza). The K562-CD137L-IL15tmb-IL-21tmb were kindly provided by Dr. Winfried S. Wels (Georg-Speyer-Haus). The K562-HLA-Ehigh were generated by overexpressing HLA-E*0.1:0.1 as a single chain construct covalently linked to b2m and to the HLA-G sequence peptide VMAPRTLFL (Gsp) at Institute for Cancer Research Oslo. HCC1954-GFP+-Luc+ were generated by lentiviral transduction using the plasmid pHIV-Luc-ZsGreen (Addgene, #39196).
Authentication	We confirmed with commercial and collaborative sources from where the cells were obtained that cell lines were authentic and free of contamination.
Mycoplasma contamination	All cell line tested negative for mycoplasma contamination prior to use.
Commonly misidentified lines (See ICLAC register)	No commonly misidentified cell lines were used.

Animals and other research organisms

Policy information about studies involving animals; ARRIVE guidelines recommended for reporting animal research, and Sex and Gender in Research

Laboratory animals	NOD.Cg-Prkdcscid Il2rgtm1Wjl/SzJ mice were obtained from Jackson laboratories (005557), 6-8 weeks old at time of intervention. All animals recruited in this study were housed in the PRBB animal housing facility with a 12 hour light/dark cycle at temperatures of 20-23°C and 40-60% humidity.
Wild animals	No wild animals were used.
Reporting on sex	All mice in this study were female
Field-collected samples	No field collected samples were used
Ethics oversight	All animal experiments were performed in accordance with protocols approved by the Barcelona Biomedical Research Park (PRBB) Animal Facility and Generalitat de Catalunya Animal Care and Use Committee (EARA-20-0045)

Note that full information on the approval of the study protocol must also be provided in the manuscript.

Plants

Seed stocks	NA
Novel plant genotypes	NA
Authentication	NA

Flow Cytometry

Plots

Confirm that:

☒ The axis labels state the marker and fluorochrome used (e.g. CD4-FITC).

☒ The axis scales are clearly visible. Include numbers along axes only for bottom left plot of group (a 'group' is an analysis of identical markers).

☒ All plots are contour plots with outliers or pseudocolor plots.

☒ A numerical value for number of cells or percentage (with statistics) is provided.

Methodology

Sample preparation	PBMC, purified NK cells by negative selection or NK cell cocultured with tumor cell lines were pre-treated with aggregated human IgG (10 µg/ml) for Fc blocking. In indirect staining, cells were incubated with hybridoma supernatants (i.e. KIRmix), washed and subsequently incubated with the corresponding secondary antibody followed by incubation with combinations of directly labelled antibodies for extracellular markers. For intracellular staining, cells were fixed and permeabilized (fixation/ permeabilization kit, BD Bioscience) and stained for intracellular antigens. All incubations were done for 20 minutes on ice. In non-fixed samples, DAPI (1 µg/ml, Sigma-Aldrich) was added prior to data acquisition as a viability dye.
Instrument	Data were acquired on FACS-Fortessa or FACS-LSRII flow cytometer (BD Bioscience)
Software	FlowJo X software (FlowJo v10.8.1,LLC).
Cell population abundance	The percentage or mean fluorescence intensities for positive cell fractions are shown in each relevant figure
Gating strategy	NK cells in PBMC samples: lymphocyte gate (FSC-H/SSC-H), single cell (FSC-H/FSC-A), alive (DAPI-), NK cells (CD56+CD3-) NK and tumor cells cocultures: lymphocyte gate (FSC-H/SSC-H), single cell (FSC-H/FSC-A), NK cells (CD56+), tumor cells (EpCAM+) or CD45-

☒ Tick this box to confirm that a figure exemplifying the gating strategy is provided in the Supplementary Information.